Soft condensed matter physics of foods and macronutrients

Soft condensed matter physics of foods and macronutrients

Salvatore Assenza[1,2] *and Raffaele Mezzenga*[1,3]*

Abstract | Understanding food properties is paramount for enhancing features such as appearance, taste and texture, for improving health-related factors such as minimizing the onset of allergies or improving the digestibility of nutrients, and for preserving food and extending its shelf-life. This Review discusses the challenges and opportunities offered by analysing foods as soft condensed matter systems. Emphasis is placed on the three main macronutrients constituting the main building blocks of foods: polysaccharides, proteins and lipids. Similarities and differences with synthetic polymers, colloids and surfactants are described. This Review also discusses the lessons that can be learned from soft matter approaches and the extent of their applicability to real foods.

Natural and processed foods are an important part of many people's heritage and cultural background. From a materials perspective, foods challenge established theoretical and experimental approaches developed to study other families of soft materials. This can be ascribed to the exceptional complexity of food systems, which is ultimately due to the heterogeneous palette of physicochemical properties displayed by their macromolecular constituents. This complexity makes foods an ideal playground for interdisciplinary research, involving physicists, biochemists or material scientists. An appealing approach to study foods is provided by soft condensed matter physics, which offers unique perspectives for interpretation of their physical properties.

From a physical point of view, foods can be regarded as highly complex soft condensed matter systems in which the properties of the final product are determined by the interplay of features corresponding to several length, time and energy scales[1]. For instance, it is common knowledge that cooking meat at high temperature results in a stiff steak. The reason for this increase in the elastic modulus involves the combined effect of the denaturation of collagen proteins (at a scale of nanometres) and their consequent aggregation into networks (at a scale of micrometres and above)[2]. More generally, the microscopic structure of foods and beverages plays a key role in their texture as perceived by the mouth[3–5].

The food microuniverse encompasses the whole field of soft matter[1], including polymer physics, supramolecular aggregation and colloidal physics, and phenomena such as spontaneous phase separation, membrane elasticity and molecular transport, across length scales from angstroms to micrometres (FIG. 1a). Improvements in experimental techniques in recent years have offered unprecedented insights into these systems, enabling refinements in food processing and the development of related biomaterials, thus providing opportunities for benchmarking the applicability of classic theories as well as for developing new physical concepts.

This Review discusses the state of the art of our understanding of foods from the perspective of soft condensed matter physics. To this end, it relies on general concepts that are not specifically related to foods, but that when applied to food may meet success, failure and new challenges. To tackle this task from the most general perspective, we focus on the main classes of macronutrients — carbohydrates, proteins and lipids — by drawing analogies (and pointing to differences) with model systems, namely polymers, colloids and surfactants (FIG. 1b). On a general level, the observed features are obtained as a compromise between entropy and enthalpy, whose relative weights are set by comparison with the thermal energy k_BT, where T is the absolute temperature and k_B is the Boltzmann constant. If the enthalpic terms are smaller than k_BT, the system is driven by fluctuations, smearing differences among states that have minimal differences in energy; in the opposite case, enthalpy and entropy both contribute to the free energy and provide the driving forces of the observed phenomena (FIG. 1b).

We first discuss the role of water as a solvent, particularly its hydrogen-bond structure and dielectric properties. Then we discuss the three main classes of macronutrients by considering their counterparts in soft condensed matter physics (FIG. 1b). In particular, we analyse the single-molecule properties of polysaccharides and unfolded proteins with the lens provided by single-polymer physics; we discuss protein aggregation by considering colloidal systems; we interpret self-organization of lipids with the aid of the physics of

Denaturation
Loss of secondary, tertiary and/or quaternary structure of a protein owing to temperature or chemical stress, for example.

[1]*Department of Health Sciences and Technology, ETH Zurich, Zurich, Switzerland.*
[2]*Departamento de Física Teórica de la Materia Condensada, Universidad Autónoma de Madrid, Madrid, Spain.*
[3]*Department of Materials, ETH Zurich, Zurich, Switzerland.*
**e-mail: raffaele.mezzenga@hest.ethz.ch*

https://doi.org/10.1038/s42254-019-0077-8

Key points

- The theoretical tools developed in soft condensed matter physics provide a means to describe foods and macronutrients at scales ranging from angstroms to tens of micrometres.
- Polymer physics can be used to characterize the properties of polysaccharides and unfolded proteins, whose complex nature poses unusual theoretical questions.
- Dispersions and gels based on proteins can be described by the physics of colloids and aggregates, and their phase diagrams can be rationalized accordingly.
- The structural properties of food emulsions and targeted delivery of macronutrients from lipid-based mesostructures can be studied and controlled with the aid of surfactant physics and transport theory.
- Some experimental soft matter tools are currently underexploited in food science, which calls for further theoretical research in soft condensed matter physics.

surfactants. In all cases, we provide examples from the world of food systems and critically review the extent to which theories can be applied, paving the way for an improved understanding of these challenging systems.

Water as a solvent

Virtually all processes involving foods take place in water-rich environments. Despite being the most common liquid on Earth, water is by far the most complex and debated one[6]. Its peculiar properties arise from hydrogen bonding, which induces short-range correlations[7] and a dynamic network of transient links between molecules[8]. Moreover, when a solute also shows a propensity for hydrogen-bond formation — which is the case for macronutrients — water solvation often leads to complex phenomena that challenge the validity of established theories (see BOX 1).

The thermodynamic anomalies of water can be understood as a consequence of a liquid–liquid phase transition at supercooled temperature[9], whose existence is debated but increasingly supported by experimental evidence[10]. Although many studies of water are experimental or simulation-based, a recent analytical model including two-body contacts, local hydrogen bonds and 12-body cooperative cages is able to capture most of the thermodynamic properties of water[11]. Many other aspects of water at extreme temperature, pressures and confinement remain to be fully explained[12].

Another important aspect of water is its role as a dielectric. At room temperature, water has a large dielectric constant ($\varepsilon \approx 80$), which has deep consequences for electrostatic interactions involving macronutrients. A large ε ensures solubility of ions by imposing a low Bjerrum length. The Bjerrum length is defined as the distance at which the bare electrostatic interaction between two elementary charges ($e_0 = 1.6 \times 10^{-16}$ C) has a magnitude equal to the thermal energy $k_B T$

$$l_B = \frac{e_0^2}{4\pi\ \varepsilon_0\ \varepsilon\ k_B T} \quad (1)$$

where $\varepsilon_0 = 8.85 \times 10^{-12}$ F m^{-1} is the absolute permittivity; in water at room temperature, this gives $l_B \approx 0.7$ nm. As discussed below, the low Bjerrum length makes ionic interactions in water particularly 'short-sighted' compared with vacuum and most other dieletrics. For example, any salt is more readily soluble in water than in alcohol or organic solvents.

Moreover, the mobile ions in solution prefentially locate around a charge of the opposite sign[13]. In this way, the overall repulsion between like charges is weakened and decays exponentially with a scale given by the Debye length

$$l_D = \frac{1}{\sqrt{8\pi\ N_A\ l_B I}} \quad (2)$$

where I is the ionic strength of the solution in mM and N_A is the Avogadro constant. To get a feeling for numbers, at room temperature water has $l_D \approx 1$ nm for $I = 100$ mM, that is, a Debye length comparable to the size of a food macromolecule. The comparability of screening length and macromolecule size has ramifications for the properties of macronutrients, both at a single-molecule level and for the formation of aggregates, as discussed below.

Single-polymer physics of macronutrients

Polymer physics is well adapted to describe macromolecular food components. Some decades ago, the pioneering work of Pierre-Gilles de Gennes[14] showed that many properties of polymer solutions depend exclusively on the string-like structure of macromolecules and on a few general features of their interaction with each other and with the surrounding solvent. Polymer physics remains a focus of active investigation, with new universal laws being uncovered in recent years[15–17].

Scaling laws. The basic description of a polymer depicts it as a chain of bonds connecting consecutive monomers. Entropy is maximized by a random orientation of bonds, but monomer–monomer and monomer–solvent interactions usually affect the final conformation of the polymer[14]. The interplay of these free-energetic contributions results in the overall size R of the chain scaling as a power-law of the polymer contour length L (FIG. 2)

$$R = C_R L^{\nu} \quad (3)$$

where ν is a universal scaling exponent and the prefactor C_R depends on the microscopic features of the polymer. Importantly, this scaling relation is valid also for subchains, so long as they are large enough to overcome effects from the intrinsic stiffness of the polymer (see below), or, to borrow from fractal language, so long as the chain portion remains self-similar. R is usually described either by the end-to-end distance R_e of the polymer or by its radius of gyration R_g, which gives the average distance between a monomer and the centre of mass of the chain[18].

The value of ν depends on the energy difference between monomer–monomer and monomer–solvent interactions. For a so-called θ-solvent, these interactions are equivalent; thus entropy dominates the free energy of the chain, and R follows random-walk statistics (the freely jointed chain model). In other words, $\nu = 1/2$ (FIG. 2a). Random-walk statistics have been reported for some food systems such as amyloid fibrils formed from the milk protein β-lactoglobulin[19] (FIG. 3a) and the

Amyloid fibrils
Protein and peptide-based fibrous aggregates with a characteristic cross-β secondary structure.

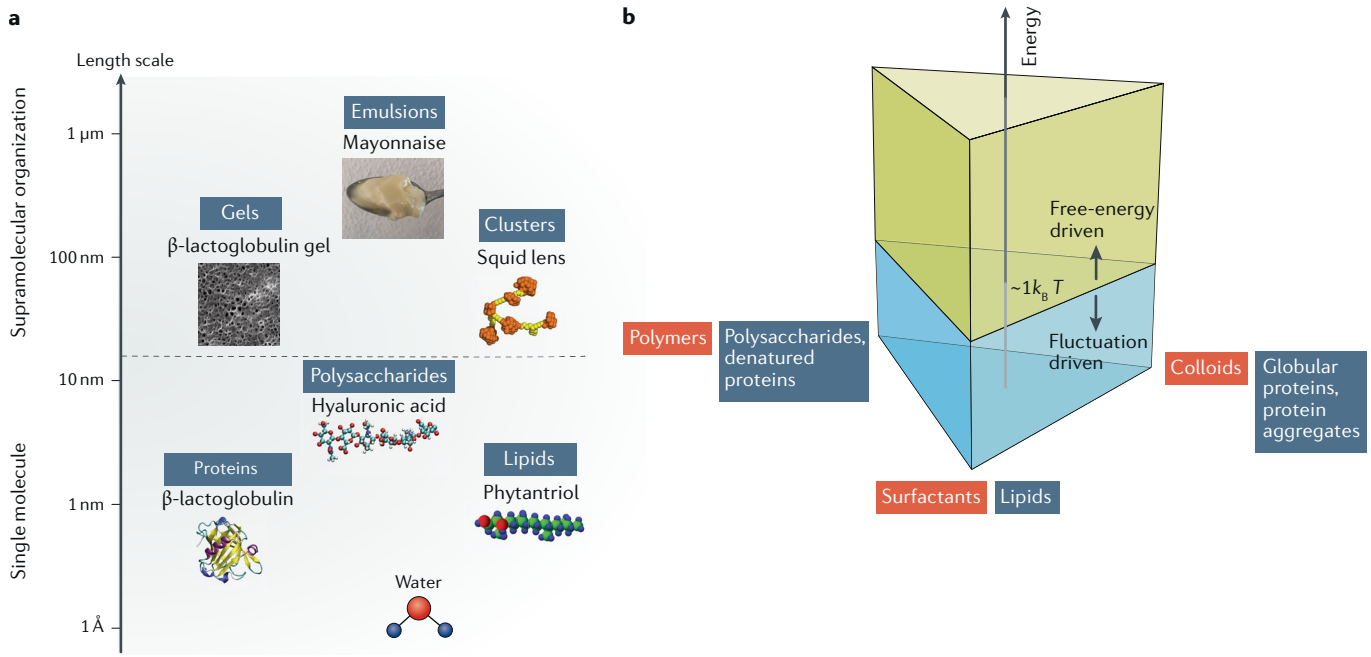

Fig. 1 | **Overview of the systems discussed. a** | The systems organized by length scale. For each class of systems (blue boxes), a representative practical example is reported (black text and images). The length scales are separated into regions of single-molecule physics (small length scales) and supramolecular assemblies (large length scales), as indicated by the horizontal dashed line. **b** | The 'magic triangle' showing the analogies between food macronutrients and soft matter model systems. The vertical axis represents the typical energy of interactions within the system. If this energy is above the thermal energy, the physics of the system is free-energy-driven; if the energy is below the thermal energy, the physics is driven by fluctuations. Panel **a** includes images reproduced with permission from REF.[182], Elsevier, and REF.[96], AAAS.

naturally occurring polysaccharide κ-carrageenan in the presence of sodium stearoyl lactylate[20], an additive used as thickener in processed foods. Nevertheless, it seems unlikely that these results stem from θ-solvent features, as this would require fine-tuned temperature and chemical conditions. As detailed below, a more refined mechanism may be at play, at least in the protein case.

For a poor solvent, monomer–monomer and solvent–solvent interactions are preferred, and the chain takes a compact conformation characterized by $\nu = 1/3$ (FIG. 2b). Moreover, at large polymer concentration, spontaneous aggregation may take place (BOX 1). Water is a poor solvent for globular proteins, as confirmed by the scaling $R_g \propto L^{0.34}$ reported for a database of thousands of proteins from the Protein Data Bank[21]. Analogously, internal subchains probed by Förster resonance energy transfer (FRET) show a scaling close to the expected value (FIG. 3b). Nevertheless, the internal structure of a folded protein is not random, because the protein is adapted for the task to be performed in vivo; thus it is expected that such internal scaling does not always hold. A compact single-protein system showing self-similarity can be obtained by denaturing a protein and putting it back into native conditions, a procedure that can result in the formation of a homogeneous globule[22], in which the protein collapses to a random compact conformation, and for which it is expected that internal scaling holds on a more general ground.

In a good solvent, monomer–solvent interactions are energetically favoured. Consequently, the polymer presents a swollen conformation characterized by monomer self-avoidance (a random coil). The extent of excluded-volume effects on chain conformation depends on the dimensionality d of the system. Flory theory yields the relationship $\nu = 3/(d+2)$ (FIG. 2c) by considering the entropy of a freely jointed chain and the overlap probability of a gas of monomers with the same concentration as the polymer system under inspection[18]. The results of Flory theory are in close agreement with values obtained from experiments and simulations in 2D and 3D, although in 3D a more precise estimation of the exponent gives $\nu = 0.588$ (REF.[23]), in agreement with renormalization-group predictions[24]. Biopolymers and food polymers are well described by the scaling laws predicted by polymer theory. For example, chemically denatured proteins closely follow the expected exponent for $d = 3$ (FIG. 3b), as shown by FRET[21] and small-angle X-ray scattering (SAXS)[25]. Similarly, at sufficiently large length scales, double-stranded DNA has $\nu = 0.59$ (FIG. 3c), as measured by strong-adsorption atomic force microscopy (AFM)[26]. Analogous results have been reported for extracts of gluten proteins[27] and polysaccharides, such as sugars extracted from lactic-acid bacteria[28] and κ-carrageenan in the presence of NaCl (REF.[20]). In 2D, the scaling behaviour of food systems such as lysozyme-based[29] and albumin-based[30] protein nanofibrils has been explored through AFM; at large length scales, the exponent matches theory (FIG. 3c).

A puzzling issue becomes evident when considering the scaling of amyloid fibrils. In 3D, β-lactoglobulin fibrils follow random-walk statistics (REF.[19]) (FIG. 3a). However, in 2D, lysozyme systems and ovalbumin

systems exhibit excluded-volume scaling[29,30]. Random-walk statistics do not change with dimensionality, and these systems are very similar to each other and in the same solvent conditions. Therefore, how is it possible that excluded-volume effects are relevant only in 2D? A possible answer relies on the way in which excluded-volume interactions decrease with the dimensionality of the system. Excluded-volume effects are relevant only when their overall strength is larger than k_BT (REF.[18]). Therefore, these effects require a minimum length L^* of

Box 1 | **Flory–Huggins theory and the challenges from hydrogen bonding**

One of the cornerstones of soft condensed matter physics is provided by the Flory–Huggins theory of spontaneous phase separation of macromolecules[18]. Based on a mean-field approximation, the free energy F of a binary mixture of a polymer and a solvent is written as

$$\frac{F}{k_BT} = \frac{\phi}{N}\ln\phi + (1-\phi)\ln(1-\phi) + \chi\phi(1-\phi) \quad (7)$$

where ϕ is the volume fraction of the polymer, N is the number of composing monomers (colloids or solvent molecules can be considered to have $N=1$) and χ is the Flory interaction parameter, representing the nature and magnitude of monomer–solvent interactions. In a good solvent, χ is small or negative, and only a mixed phase is present. In a poor solvent, $\chi>0$ and spontaneous phase separation may occur: above the binodal line, a biphasic system is thermodynamically stable; between the binodal and spinodal lines, the mixed phase is metastable, and phase separation occurs through nucleation and growth; above the spinodal line, a rapid phase-separation process, known as spinodal decomposition, takes place without energy barrier (see the figure, panel **a**). The temperature dependence of χ is usually well described empirically by $\chi=A+B/T$. Usually, $B>0$, that is, χ decreases for increasing temperature. In this case, the $\phi-T$ phase diagram is qualitatively the vertically mirrored image of the $\phi-\chi$ diagram. Therefore, the $T(\phi)$ binodal is an upper critical solution line (UCSL), that is, phase separation occurs only below it. In some other cases, $B<0$, and a lower critical solution line (LCSL) is instead found, that is, the $\phi-T$ phase diagram is qualitatively similar to the $\phi-\chi$ one.

Short, neutral, water-soluble polymers, such as polyethylene glycol and many neutral food polysaccharides (experimental data for polyethylene glycol molecules shown as points in panel **b** of the figure), show closed-loop solution lines (CLSLs), that is, phase separation occurs only within a limited region (theoretical predictions shown as lines in panel **b** of the figure). This finding is predicted by an extension of Flory–Huggins theory[177], in which the presence of clusters (see the figure, panel **c**) accounts for the possibility of hydrogen bonding. In this model

$$\frac{F}{k_BT} = \phi_0\ln\phi_0 + \sum_{m=0}^{f}\frac{\phi_{m+1}}{N+m}\ln\phi_{m+1} + \chi\phi(1-\phi) \quad (8)$$

where ϕ_0 is the volume fraction of unbound water, ϕ_1 is that of unbound polymers and ϕ_{m+1} is that of m-clusters, that is, clusters consisting of a polymer plus m bound water molecules; f is the maximum number of bound water molecules that can be accommodated on the polymer; and $\phi=\sum[N/(N+m)]\phi_{m+1}$ is the total volume fraction of the polymer clusters. Imposing chemical equilibrium among the clusters leads to $\phi_{m+1}=K_m\phi_1\phi_0^m$, where K_m is a decreasing function of temperature. Assuming $B>0$, temperature has two effects on the phase behaviour of the system. To start, the Flory–Huggins parameter decreases with increasing temperature, leading to the appearance of UCSLs. In parallel, however, increasing temperature disrupts hydrogen bonds, making the solvent poorer and qualitatively acting like the case $B<0$, promoting a phase diagram with LCSLs. For sufficiently short chains, these two effects compete, and a CLSL appears. For larger polymers, the biphasic region increases in size, and for long chains only the LCSL is present. This model precisely captures the experimental data (panel **b**) and shows the importance of polymer–water hydrogen bonding for features beyond the reach of the classic Flory–Huggins theory. This framework has successfully rationalized the phase diagrams of various food systems, including methylcellulose[178] and hydroxypropyl cellulose[179].

Other expansions to the Flory–Huggins model have been proposed to describe the features of membraneless organelles in cells, particularly considering the presence of charges and heteropolymers[106,180,181]. These examples show the limits of classical theories in describing real systems, and the importance of feedback from experiment to improve theoretical understanding. Panel **b** is reproduced with permission from REF.[177], APS.

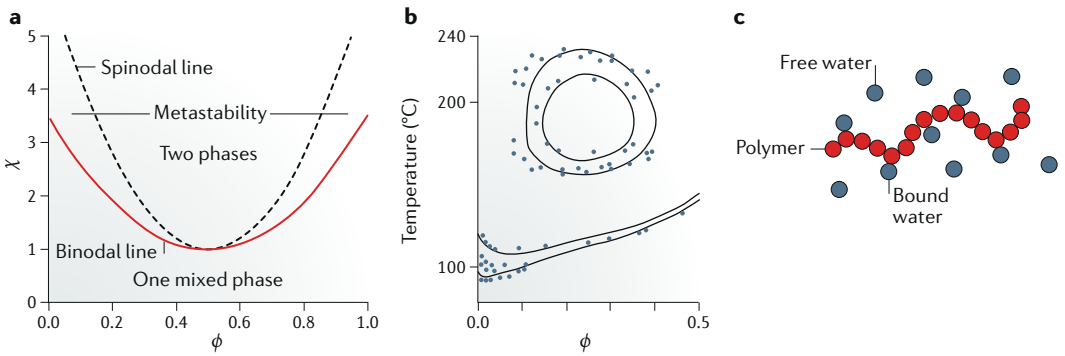

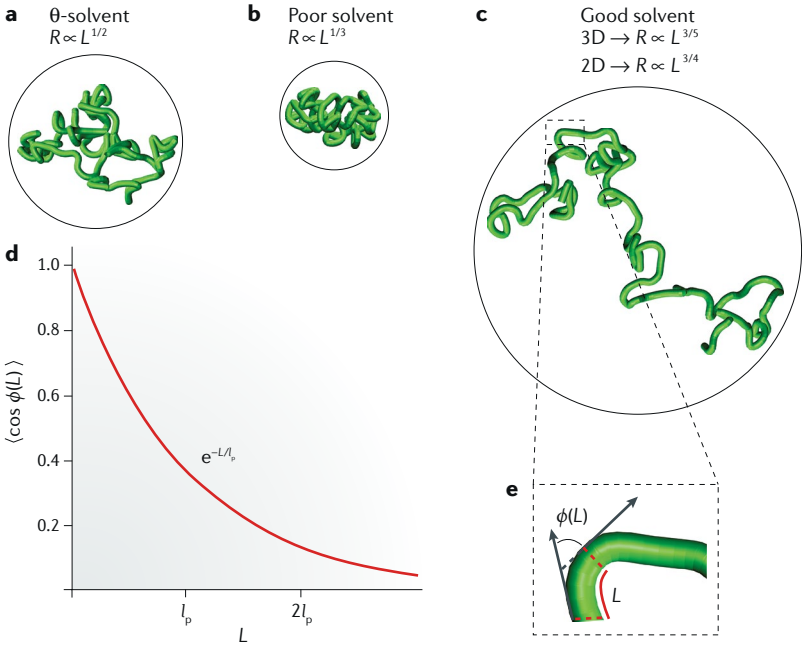

Fig. 2 | **Definitions of single-polymer physics. a** | Typical conformation of a polymer in a θ-solvent, for which the overall size R of the polymer (indicated by the circle) scales as its contour length L to the power of 1/2. **b** | Typical conformation of a polymer in a poor solvent. The conformation is more compact than that in a θ-solvent, and the scaling exponent is correspondingly reduced to 1/3. **c** | Typical conformation of a polymer in a good solvent. Flory theory indicates that in this case the scaling exponent depends on the sytem dimensionality. In panels **a**–**c**, all polymers have the same contour length. **d** | The bond correlation function $\langle \cos \phi(L) \rangle$ decays exponentially with characteristic length scale equal to the persistence length l_p. $\langle \ldots \rangle$ denotes statistical average, and $\phi(L)$ is the angle between two vectors tangent to the polymer and separated by L (as indicated in panel **e**). **e** | Zoom-in on part of panel **d**.

the polymer to ensure enough monomer–monomer contacts. Because random encounters between monomers are more likely in 2D than 3D, a smaller threshold length is expected: $L^*_{2D} < L^*_{3D}$. Thus, it is possible that the contour lengths of amyloid fibrils lie between these two threshold values. Dedicated work is needed to conclusively solve this issue, for instance by considering the concept of a thermal blob, which provides an estimate of L^* based on Flory arguments[18]. In the present context, this problem epitomizes the challenges posed by food systems to well-established soft matter theories.

Polymer rigidity. The scaling picture is further enriched when looking at short subchains, for which $\nu = 1$ (FIG. 3c). The reason behind this behaviour is that the length scales considered are below the persistence length l_p of the polymer, which is related to its bending rigidity. l_p is defined as the characteristic length of the exponential decay of the bond–bond correlation function (FIG. 2d) and indicates how long a chain is needed to observe thermally induced bending (FIG. 2e). At length scales shorter than l_p, the polymer is practically a stiff rod, which imposes $R \propto L$, that is, $\nu = 1$. l_p depends on the Young's modulus of the constituent material, the cross-section of the chain and temperature. Typical values encompass many orders of magnitude, from a few angstroms for proteins[31] to millimetres for microtubules[32].

For amyloid fibrils based on the food proteins β-lactoglobulin, lysozyme and serum albumin, l_p has been reported to be 1–4 μm, depending on the number of protofilaments composing the fibrils[29,30,33]. Bundles of β-lactoglobulin fibrils cross-linked by pectin nanoparticles also have similar persistence lengths[34]. However, different cross-linking mechanisms are expected to yield heterogeneous values of l_p, owing to the corresponding effective cross-section of the bundle, so these results are not generally applicable to all fibril bundles. It is worth highlighting how processing conditions in food may lead to changes in l_p by four orders of magnitude, from native proteins[31] to their fibrillar form once denatured and hydrolysed[29,30,33].

In contrast, the variation in persistence length of polysaccharides depends primarily on the particular macromolecule considered. For instance, l_p values of 5–10 nm have been reported for polysaccharides from lactic-acid bacteria[28]. In the case of xanthan, different strains of the producing bacteria yield $l_p = 30$–80 nm, owing to differences in chemical details and the presence of secondary structure[35]. A similar range of variability has been reported for amylose in various solvents[36–39], in which monomer–solvent hydrogen bonding can induce a two fold increase in rigidity[37]. Finally, values of 10–60 nm have been reported for carrageenans, depending on chemical details, secondary structure and salt conditions[40,41]. On a general level, the fundamental mechanisms linking the details of a polysaccharide to its persistence length depend on the chemical structure of the backbone, possible secondary structures, salt conditions and specific interactions, so that general trends on polymer rigidity remain highly system-specific.

Polyelectrolytes. The physics of charged polymers is of particular relevance for food systems, especially for polysaccharides, which in most cases host charged groups along the chain. Theoretical and experimental research on polyelectrolytes is one of the most active areas of research in polymer physics[42]. This activity is also due to the lack of a unified theoretical framework capable of describing the whole phenomenology, in contrast with other well-developed branches of polymer science. Although the scaling laws considered above still hold for charged polymers, the interaction between charges induces substantial modifications to chain flexibility.

Owing to the presence of counterions, the interaction between two charges separated by a distance r is screened according to the Debye–Hückel potential[13]

$$U_{el} = k_B T \left(\frac{l_B}{r} \right) e^{-\frac{r}{l_D}} \quad (4)$$

where l_B is defined in equation 1 and l_D is defined in equation 2. The electrostatic repulsion between charges along the chain increases the stiffness of the polymer, which is usually accounted for by treating the persistence length as $l_p = l_p^0 + l_p^{el}$, where l_p^0 is the contribution from the intrinsic stiffness and l_p^{el} is the contribution from electrostatic interactions. The dependence of l_p^{el} on the ionic strength of the solution has been the focus of some

Thermal blob
The portion of chain length whose total interaction energy is of the order of $k_B T$.

Hydrolysed
When peptide chains are fragmented into shorter subunits by chemical, enzymatic or thermal stimuli.

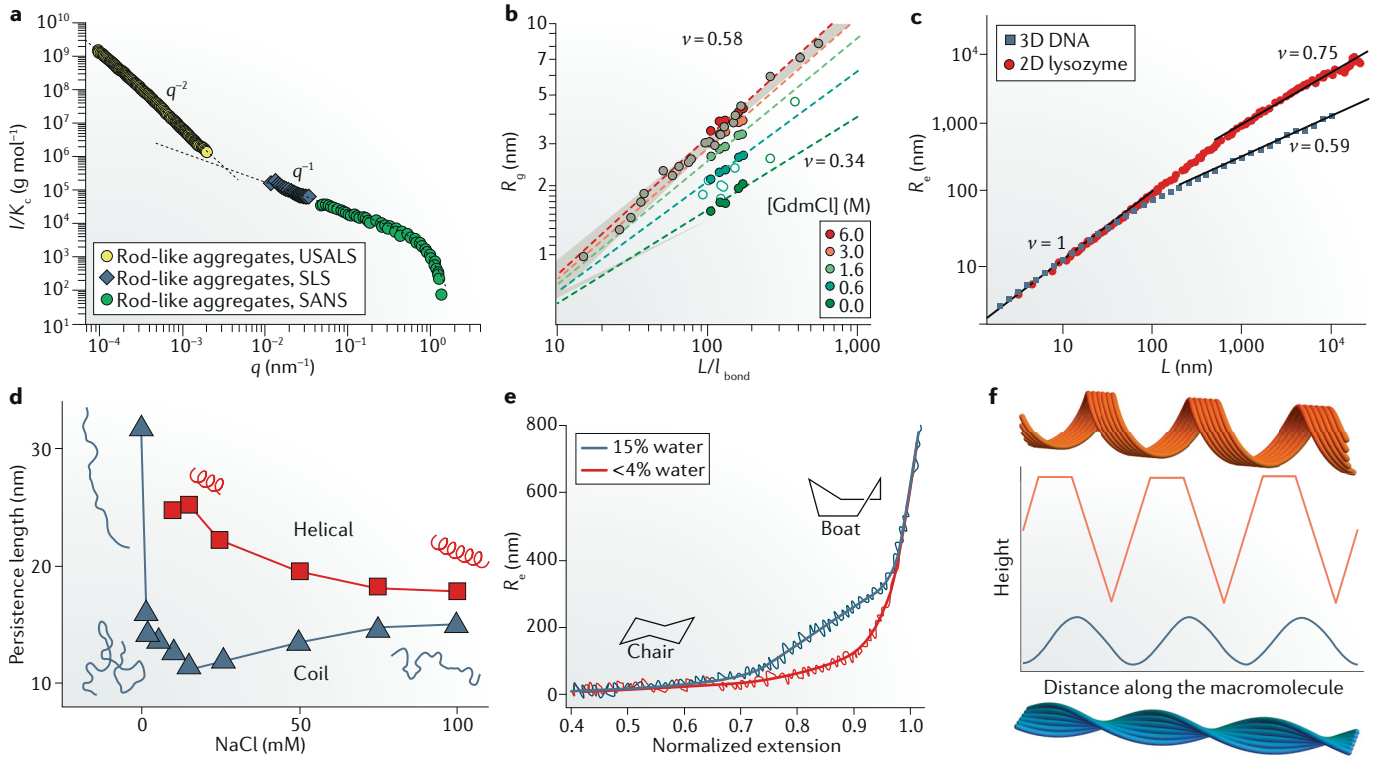

Fig. 3 | **Applications of single-polymer physics concepts to protein systems and polysaccharides. a** | Scattering intensity profile I versus magnitude of scattering vector q for a solution of amyloid fibrils produced from β-lactoglobulin. The scaling exponent relating I and q for small q is the inverse of the single-molecule exponent $\nu = 0.5$. The q value at the intersection of the two fits is proportional to the inverse of the persistence length. **b** | Radius of gyration R_g versus internal contour length L (rescaled by the bond length l_{bond}) for proteins at various denaturant concentrations measured by FRET (Förster resonance energy transfer; coloured dots) and small-angle X-ray scattering (grey and open dots). As the denaturant concentration increases, the system passes from poor solvent conditions (indicated by $\nu = 0.34$) to good solvent conditions (indicated by $\nu = 0.58$). **c** | Scaling regimes of the end-to-end distance R_e versus L below and above the persistence length, for double-stranded DNA in 3D (blue squares, data from REF.[26]) and lysozyme fibrils in 2D (red circles, data from REF.[29]). **d** | Persistence length versus concentration of NaCl for carrageenan chains in both coil and helical secondary structure conformations. Coil conformations show non-monotonic behaviour, which is not captured by current polyelectrolyte theories. The insets indicate typical configurations. **e** | Force-versus-extension curve for amylose at different hydration levels, together with the fit from a modified freely jointed chain that includes the presence of boat and chair configurations (insets). The upper curve corresponds to large hydration of the sample; the lower curve corresponds to low hydration. At sufficiently high hydration, a transition from chair configuration to boat configuration is observed upon pulling. **f** | Cartoons of amyloid fibrils with secondary structures arranged according to a helical ribbon (top, orange) and a twisted ribbon (bottom, cyan). The corresponding idealized height profiles, as would be measured by an atomic force microscope tip, provide a 'fingerprint' to recognize the structure under study. GdmCl, guanidinium chloride; SANS, small-angle neutron scattering; SLS, static light scattering; USALS, ultra-small-angle light scattering. Panel **a** is reproduced with permission from REF.[19], ACS. Panel **b** is adapted with permission from REF.[21], PNAS. Panel **d** is adapted with permission from REF.[40], ACS. Panel **e** is adapted with permission from REF.[65], ACS.

debate. The classic theory of Theo Odijk[43], and Jeffrey Skolnick and Marshall Fixman[44] (OSF theory) treats the polymer conformation as a perturbation from a straight rod. From there, the cost in electrostatic energy induced by bending can be computed; the electrostatic contribution to the persistence length was shown to behave as $l_p^{el} \propto l_D^2 \propto 1/I$. Nevertheless, this dependence on ionic strength reproduces only the experimental data for stiff polymers[45], such as double-stranded RNA[46], and some doubt has been casted on the applicability of OSF theory for double-stranded DNA[47,48]. For flexible polymers, a variational approach predicts a weaker relation[45]: $l_p^{el} \propto l_D \propto 1/\sqrt{I}$, which has been observed in flexible polymers, such as single-stranded DNA[49]. Despite their experimental validation in a number of systems, both these theories have been challenged by simulations, for which a bead-spring model polymer gives a sublinear dependence $l_p^{el} \propto l_D^{\gamma}$ ($\gamma < 1$)[50].

Experiments on food systems have also challenged the theoretical results. For instance, systematic force-spectroscopy experiments on the carbohydrate polymer hyaluronic acid at different ionic strengths reveal an intermediate scaling law $l_p^{el} \propto I^{-0.65}$ (REF.[16]). The data from these experiments collapse onto a master curve upon a suitable rescaling of force and extension, indicating an underlying universal law. Although the physical origin of this universality is still an open question, simulations based on the Debye–Hückel potential reproduced

the collapse of data, supporting the existence of a general law of polymer physics[15]. The behaviour of carrageenans is even more puzzling[40]. At low and intermediate ionic strengths, l_p^{el} shows a sublinear dependence on l_D, in line with the simulation results of REF.[50] but in contrast to theoretical predictions. Furthermore, for a group of observed molecules the persistence length shows a non-monotonic dependence on ionic strengths, and after a turning point it becomes an increasing function of I (FIG. 3d). Current theories are unable to explain this non-monotonic behaviour, and it is to be hoped that experimental work will spark interest among theoretical and numerical soft condensed matter scientists.

Another interesting feature of polyelectrolytes is provided by counterion condensation, first predicted by Gerald Manning[51]. Owing to the approximate cylindrical symmetry of a polymer, when the linear charge density exceeds a critical value the gain in electrostatic energy from counterion localization near the chain overcomes the loss in translational entropy. For monovalent ions, the result is a massive condensation phenomenon[52]. Manning condensation occurs when the distance between consecutive charges is less than the Bjerrum length and the number of counterions involved is such that the final effective linear charge density corresponds to an average spacing of l_B between unit charges. Manning condensation affects the properties of the polymer. For instance, molecular dynamics simulations have shown the key role played by this mechanism in determining the electrophoretic mobility of homogalacturonans[53]. Moreover, accounting for counterion condensation leads[54] to a prediction for the electrostatic contribution to the persistence length $l_p^{el} \propto I^{-0.7}$. This exponent is in line with the experimental results on hyaluronic acid[16]. Nevertheless, simulations based on Debye–Hückel theory[15] (which by construction cannot show Manning condensation) also reproduce the correct exponent; thus other mechanisms are expected to be behind this result. In the case of carrageenans, Manning condensation could not account[40] for the observed behaviour of l_p^{el} at any level. Quantitatively, the theoretical exponent is too large. Qualitatively, the non-monotonicity remains a mystery. Furthermore, it was also observed that carrageenans with linear charge density both below and above the critical threshold show similar behaviour, thus calling into question the relevance of Manning condensation for the determination of the properties of food systems and suggesting a role for ion-specific interactions[40], a feature that is not accounted for in classical polyelectrolyte theories.

Force spectroscopy. The response of a single polymer to an external pulling force provides invaluable information on the elastic properties of the chain. These properties can be extracted by fitting the smooth segments of the force-versus-extension curve (FEC) with appropriate formulae from polymer physics[18,55] (FIG. 3e), enabling an alternative route to evaluate the persistence length of the chain. Moreover, the presence of complex structures within a polymer chain can be identified via rupture events, in which the FEC shows a sudden extension corresponding to force relaxation. Force spectroscopy has proven to be a versatile and reliable method to assess the single-molecule properties of biomolecules from its early days[56–58] and is today a key tool in biophysics[59–61], providing an unprecedented level of detail on molecular processes and related free energies[62], as well as an ideal testing ground for new theories[63]. In the case of polysaccharides, force spectroscopy has not yet been exploited to its full potential[61,64], in spite of an encouraging start, in which a pioneering work investigated the elastic response of the polysaccharide dextran using AFM pulling[58]. There are, however, some notable exceptions to this trend[16,34,65–67]. For instance, a recent investigation focused on the response of amylose to an external pulling force[65]. The observed FECs (FIG. 3e) could be rationalized by considering a freely jointed chain in which each monomer could switch between two states corresponding to different atomic arrangements of the sugar ring, known as chair and boat configurations. The role of water on the conformational properties of amylose was assessed by performing several pulling experiments in the presence of water and propanol in different proportions, which enabled computation of the difference in free energy between the two states as a function of water content. Our hope is that this work will inspire further investigations of polysaccharides based on force spectroscopy, which is envisaged to give access to molecular details and have a considerable impact on food biotechnology.

Secondary structure. The development of single-molecule techniques has fostered research probing the structural features of food macromolecules by direct visualization, for instance, by transmission electron microscopy or AFM. AFM imaging in particular has proved to be a powerful tool, enabling the verification of proposed structural models by measuring the height profile along a molecule deposited on a substrate. For instance, amyloid fibrils based on β-lactoglobulin and lysozyme have been shown to arrange as purely twisting or purely bending ribbons, according to their width[33,68]. These two geometrical arrangements can be distinguished using their height-profile fingerprints (FIG. 3f). In the case of twisting ribbons, the twisting periodicity is related to the width of the ribbon via a universal law[69], which also captures the behaviour of some fibrils unrelated to food systems[70].

Examples involving polysaccharides comprise investigations on the heterogeneous conformation of xanthan, including single-stranded coils and double-stranded branched structures or helices[35,71]. Analogous studies have evidenced the existence of helical structures in xyloglucan[72] and triple-stranded bundles in curdlan[73]. In the case of carrageenans, the coil–helix transition was studied[41], together with its dependence on the salt added to the solution[40] and the formation of aggregates of higher order[74]. The observation of ion-specific features among monovalent salts (KCl, NaCl) contrasts with standard soft matter physics models, which predict (via the Poisson–Boltzmann equation[13]) the behaviour of the system to depend only on the valency of the counterions. This example provides a further case of food systems being more complex than standard soft matter theories.

Globular proteins, colloids and aggregates

When considering larger length scales and polymer concentrations than those discussed above, the role of intermolecular interactions in determining the physical properties of food systems is as important as — if not more important than — that of individual polymer properties.

For instance, it is well known that globular proteins in solution tend to attract each other, leading to spontaneous phase separation[75]. The experimental phase diagrams derived for a number of protein systems show liquid, gel or crystal phases, resembling those obtained for colloidal solutions[76], which are more easily tackled both theoretically and experimentally. The physics of colloids is thus appropriate for qualitatively — and sometimes quantitatively — describing the mechanisms underlying the behaviour of protein systems.

Isotropic potentials. The simplest approach treats proteins as spheres of radius R interacting via an isotropic potential $U(r)$, that is, a potential depending only on the mutual distance r. In this regard, the classic Derjaguin–Landau–Verwey–Overbeek (DLVO) theory is the standard theoretical framework[13,75] (FIG. 4a)

$$U(d) = \frac{8\pi^2\sigma^2 R l_D^2 l_B}{e_0^2} k_B T \, e^{-\frac{d}{l_D}} - \frac{A\,R}{12d} \quad (5)$$

where $d = r - 2R$ is the minimum distance separating the surfaces of the colloids, σ is the surface charge density, e_0 is the elementary charge and A is the Hamaker constant of the colloid. The first term on the right-hand side of equation 5 gives the electrostatic repulsion between two like-charged spheres in the Debye–Hückel approximation (compare with equation 4, which holds for point-like particles); the second term is the van der Waals attraction. $U(r)$ has an infinite well at $d \to 0$, which captures the tendency of colloids to aggregate (FIG. 4a). To reach this stable aggregated state, the colloids must overcome a barrier whose height increases with R and decreases with I. In the case of proteins (R on the scale of nanometres), this height is of the order of $k_B T$ (FIG. 4a), implying that thermal fluctuations alone can trigger aggregation[75]. The DLVO theory is customarily used to rationalize experimental data, such as measurements of the second virial coefficient of lysozyme solutions from light-scattering data[77,78]. Nevertheless, it is by no means the only choice. Other popular models include the Baxter model[79], characterized by a short-range attraction in contrast to DLVO[75]; depletion interactions[80,81], in which attraction is induced by the presence of co-solvents, which maximize their translational entropy when the colloids are in proximity to each other; or simple square well potentials, which are often preferred for practical convenience[82–85].

All such potentials introduce severe approximations, and it is not clear to what extent they can be applied to protein systems. In this regard, a more general theoretical framework is provided by the extended law of corresponding states[86]. According to this law, for any isotropic potential, the thermodynamic properties of the solution are universal once the variables are rescaled by three characteristic scales: attraction energy, hard-core repulsion length and potential range as quantified by the second virial coefficient. Consequently, the existence of a master curve for binodals and spinodals (see BOX 1 for their definition) has been shown for simulation data for several colloidal potentials[77,78,87]. Experimental data also fall onto a master curve but can be reconciled with simulation results based on isotropic potentials only if temperature-dependent attraction wells are considered[77,84].

Proteins as patchy colloids. An important feature overlooked by the above-mentioned isotropic potentials is the heterogeneity of protein surfaces, which contain patches with different charges or hydrophilicity (FIG. 4b). This results in anisotropic protein–protein interactions, as evidenced by the specific molecular orientations observed in protein crystals[76]. A more refined approach that tackles this issue is the theory of patchy colloids, in which proteins are modelled as spheres with sticky patches on their surface[88] (FIG. 4b). The features of the phase diagram are primarily affected by the number of patches per colloid and integral properties such as the second virial coefficient, but are rather insensitive to the details of the potential[75]. The theory of patchy colloids has been successfully used to quantitatively reproduce the phase diagram of protein systems such as lysozyme and γ-crystallin[89,90], thus providing a key advance over isotropic potentials (FIG. 4c). Moreover, it has been shown that the extended law of corresponding states can be extended to patchy systems[91], thus explaining its success in describing protein systems beyond the simplistic original approximation of isotropic potentials.

Patchy colloids are now widely used to interpret experimental findings[92–98]. In parallel, they remain an active field of theoretical research[99], with focus on questions such as the interplay of anisotropy and electrostatics[100,101] or effective interactions induced by patchy co-solvents[102]. In addition, dynamic phenomena are being investigated, such as the impact of anisotropic interactions on association kinetics[103] and on the diffusive properties of the system[94,104].

Protein aggregates. Under the right conditions, the presence of attractive interactions can lead to the formation of protein aggregates. Many aggregation pathways have been identified, and the final features of the clusters depend strongly on the particular protocol considered, such as increase in concentration, thermal denaturation or acidic stress. This section will focus on a few illustrative cases; a more thorough discussion can be found in reviews dedicated to the topic[75,105–107].

The interplay of short-range attraction and long-range repulsion, which are the main ingredients of the potentials considered in the previous sections, was theoretically predicted to lead to the formation of clusters of colloids[108] and experimentally reported for native lysozyme[109], bovine serum albumin[110] and ovalbumin[111]. In particular, SAXS measurements showed two peaks in lysozyme systems, which were ascribed to cluster–cluster (low-q, where q is the size of the scattering vector) and

Hamaker constant
A quantity with the units of energy characterizing the van der Waals interactions between colloids.

Second virial coefficient
A quantity with units of volume describing the net two-body interactions between two particles; positive and negative values indicate net repulsion and attraction, respectively.

Association kinetics
Dynamic features of binding between particles, usually characterized by suitable rate constants.

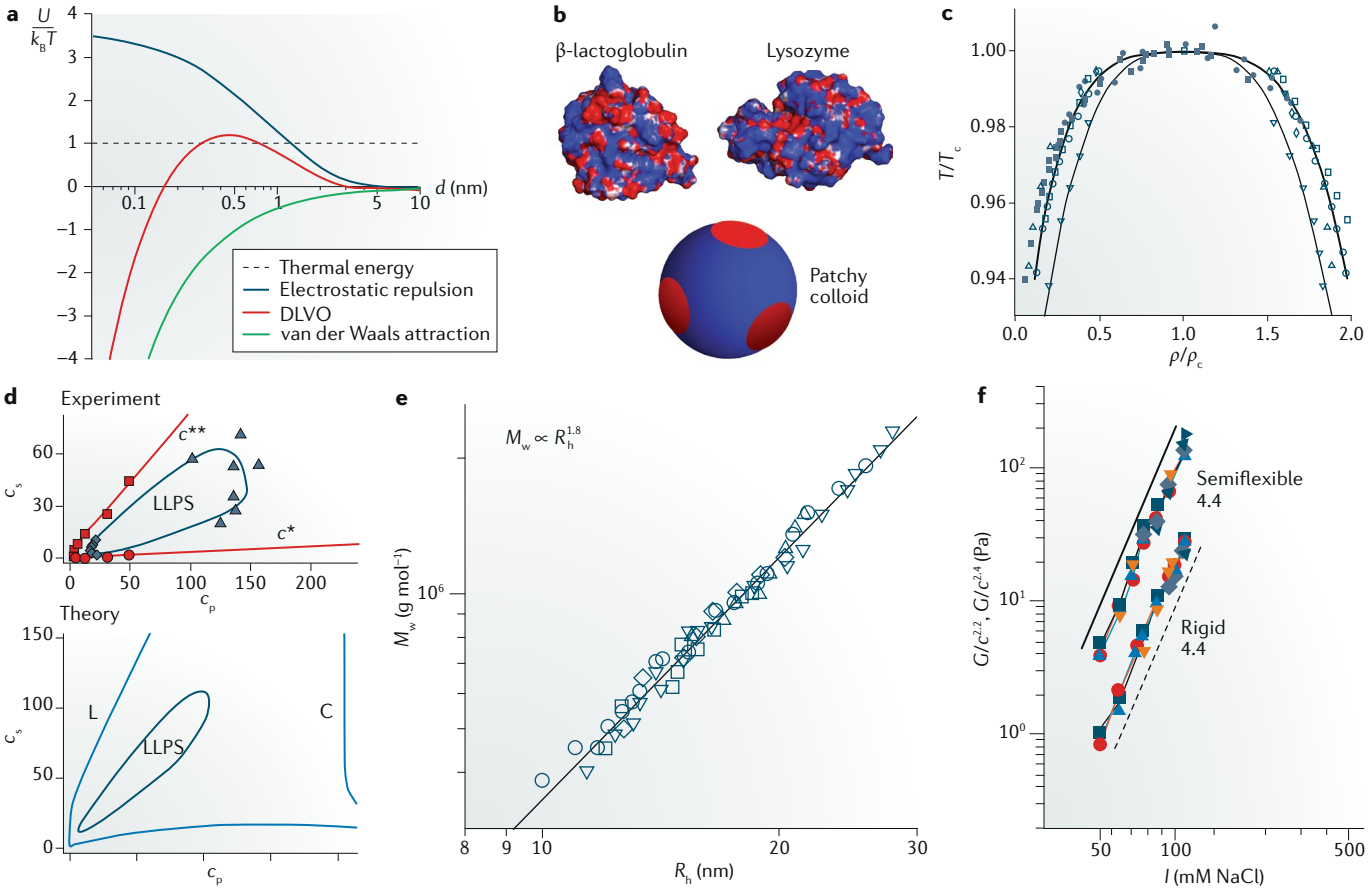

Fig. 4 | **Physics of colloids and aggregates applied to food systems. a** | Representative plot of the interaction energy U scaled by thermal energy k_BT at room temperature, as a function of colloid separation d for a DLVO (Derjaguin–Landau–Verwey–Overbeek) potential (equation 5), for a protein system. The DLVO potential is a superposition of van der Waals attraction and electrostatic repulsion. The height of the aggregation barrier, which arises from electrostatic repulsion, becomes comparable to the thermal energy in globular proteins at room temperature. **b** | Patchy features of food proteins and example of a patchy colloid. In the case of proteins, the images show the charge distribution (red and blue indicate negatively charged and positively charged spots, respectively) obtained starting from the crystallographic structures (1BEB for β-lactoglobulin[183] and 1DPX for lysozyme[184]) by means of the PBEQ solver[185]. **c** | Phase diagram of protein systems and models. The temperature T and density ρ are rescaled by their values at the critical point (T_c and ρ_c, respectively), identified as the maximum of the binodal. The binodal curve for γ-crystallin and lysozyme (filled circles and squares, respectively) collapses onto the same master curve as patchy models (open squares and circles), whereas isotropic fluids behave differently (open triangles). **d** | Experimental phase diagram of solutions of human serum albumin in the presence of YCl_3; a patchy model with transient bonds reproduces the qualitative features of the phase diagram. **e** | Power-law dependence of the mass M_w of a soy-globulin aggregate on its hydrodynamic radius R_h indicates a self-similar structure, characterized by a fractal exponent $d_f \approx 1.8$. **f** | After rescaling by a suitable power of the concentration c (power exponents of 2.4 and 2.2 refer to rigid and semiflexible cases, respectively), the storage modulus G_0 of gels based on β-lactoglobulin amyloid fibrils is a universal function of the ionic strength I of the solution, in close agreement with a theory combining the affine thermal model and DLVO. Different symbols correspond to different concentrations. c*, c**, threshold salt concentrations; C, crystal phase; c_p, protein concentration; c_s, salt concentration; L, homogeneous-liquid phase; LLPS, liquid–liquid phase separation. Panel **c** is reprinted from REF.[89], with the permission of AIP Publishing. Panel **d** is adapted from REF.[98], Springer Nature Limited. Panel **e** is adapted with permission from REF.[126], Elsevier. Panel **f** is reproduced with permission from REF.[134], APS.

intra-cluster (high-q) interactions[109]. The position of the low-q peak was independent of protein concentration, suggesting a constant number of clusters of increasing size, in agreement with theory[108]. Nevertheless, the interpretation of data was controversial enough to lead to a yet-unresolved[106] debate in which the very existence of clusters was questioned[112–114], although more recent works seem to reinforce their presence[115,116]. In the same system, the concentration dependence of short-time diffusion and viscosity has been assessed[117], showing that quantitative agreement between theory and experiments is lost at high lysozyme concentration, thus calling for further theoretical research. Small-angle neutron scattering (SANS) has been used to study how attractive and repulsive interactions depend on ionic strength, protein concentration and temperature[118]. A sudden change in SANS profiles occurs beyond a critical temperature, at which thermal denaturation occurs and a different aggregation pathway of proteins becomes dominant, as discussed below.

Patchy-colloid physics has successfully explained the behaviour of several proteinaceous aggregates.

Isoelectric point
Value of pH for which partial protonation induces a net zero charge in a molecule hosting several positively charged and negatively charged groups.

Storage modulus
Parameter with the units of pressure quantifying the elastic response of a viscoelastic material to an external stress.

Block copolymers
Macromolecules obtained by covalently joining two polymers with different physico-chemical properties by one end.

For instance, it formed the basis for simulations that captured the experimentally observed features of gels of S-crystallin proteins in the squid eye lens, as well as albumin in pidan egg and monoclonal antibodies[95,96,119]. Analogously, the experimental phase diagram of human serum albumin in the presence of the salt YCl_3 was nicely reproduced by a patchy particle model[98]. At a given protein concentration c_p, experiments reveal a re-entrant phase transition when varying the salt concentration c_s, bound by the threshold values c^* and c^{**} (FIG. 4d). Outside this range, a homogeneous solution is found; for $c^* < c_s < c^{**}$, condensation is observed. Within this region, a closed-loop inner region is further observed, where metastable liquid–liquid phase separation takes place. This complex phase diagram was nicely captured by a patchy model in which the trivalent ion Y^{3+} could transiently bind on specific spots on a protein and provide a sticky interaction with other proteins via salt bridges (FIG. 4d).

Protein aggregation following thermal denaturation is especially relevant for food systems, as it is directly related to gelation processes in cooking eggs[120] and meat[2,121], for example. Similarly, aggregation induced by mild acidification is relevant for systems such as yoghurt[122]. As the globular structure is lost, proteins expose hydrophobic patches that promote the formation of contacts between the denatured proteins. The fractal gel model[75] considers the aggregate as a self-similar object characterized by a size $\xi \propto M^{1/d_f}$, where M is the mass and $1 \leq d_f \leq 3$ the dimensionality of the cluster. $d_f = 1$ corresponds to filamentous aggregates, such as amyloid fibrils, and is typically obtained by hydrolysing the protein under extreme conditions of temperature and pH[19]. Below the percolation threshold, aggregates corresponding to simple denaturation usually yield $d_f \geq 1.7$ (REF.[75]). For instance, β-lactoglobulin systems at low ionic strength exhibit $d_f = 1.7$ (REF.[123]), whereas stronger salt screening yields a more compact structure ($d_f = 2$)[124]. Ovalbumin behaves in a similar manner on varying pH[125]: more compact gels are observed closer to the isoelectric point, that is, for lower electrostatic repulsion. Soy globulin has $d_f = 1.8$ (REF.[126]) (FIG. 4e). Gluten proteins exhibit $d_f = 2$ both for proteins dissolved in water/ethanol mixtures and for deuterated water[27,127,128]. Aggregation of complexes of polysaccharides and proteins has been recently analysed[129], yielding a fractal dimension in line with the results reported for proteins ($d_f = 1.9$).

The fractal gel model also predicts the rheological properties of the gels obtained by aggregation. A scaling argument based on entropic considerations predicts the storage modulus[130] $G \sim k_B T/\xi^3$. The argument assumes that the gel percolates the system with ξ as the mesh size: that is, the smallest scale at which the self-similarity can be present. Because self-consistency on local and global concentration C imposes $\xi \propto C^{1/(d_f-3)}$, this leads to the scaling $G \propto C^{3/(3-d_f)}$. Another model is based on enthalpic contributions from the connecting chains which, when present, are predicted to give a stronger exponent, namely $G \propto C^{(3+d_b)/(3-d_f)}$, where d_b is the fractal dimension of the connecting chain[131]. Using the value measured from light scattering ($d_f = 2$, see above), analysis of the storage modulus for β-lactoglobulin gels gives[124] $d_b = 1.5$. Similarly, gels based on basil seed gum yield[132] $d_f = 2.3$ and $d_b = 1.2$.

The main drawback of the fractal gel model is in its limited account of the polymer physics of the connecting chains. More refined models exist in the literature but have not found wide application in studies on food-related systems. For instance, the affine thermal model includes the effects of crosslink length of the network (l_c) and persistence length of the constituting polymers[133]

$$G \sim k_B T \frac{l_p^2}{\xi^2 l_c^2} \tag{6}$$

Recently, this model was combined with the DLVO potential to assess the dependence of G on ionic strength I for networks of amyloid fibrils based on β-lactoglobulin and lysozyme[134]. The predicted power laws were $G \propto I^{4.4}$ for β-lactoglobulin (FIG. 4f) and $G \propto I^{3.8}$ for lysozyme. These values closely match experimental results, thus showing the power of polymer-based predictions for food gels.

Physics of lipids

The third pillar of the soft condensed matter physics of macronutrients is provided by surfactants, which are a good model for the behaviour of lipids in presence of water. Notable food examples are given by the microscopic structural evolution of edible emulsions rich in fat content under digestion, such as cow milk[135], human breast milk[136] and mayonnaise[137].

Flory–Huggins considerations. At a general level, surfactants are amphiphilic macromolecules, that is, the two ends interact differently with the solvent. As a result, the system tends to maximize the number of contacts between the solvent and the molecular end with more affinity and minimize the number of contacts at the end with less affinity. This tendency may easily result in microphase separation. Useful considerations come from applying the Flory–Huggins theory (BOX 1) to lipids and to the model system provided by block copolymers. In Flory–Huggins theory, spontaneous microphase separation takes place when $\chi N > 10.5$, where χ is the Flory–Huggins parameter and N the number of statistical segments in the polymer[138]. For block copolymers, $\chi \approx 0.1$ (REF.[139]), and thus a relatively large $N \approx 100$ is needed for phase separation to occur. Assuming the same criterion for phase separation also holds in lipids, where large enthalpy leads to $\chi \approx 3$, the condition $\chi N > 10.5$ implies that values as low as $N = 4$ are sufficient for witnessing phase separation, a condition easily fulfilled for most lipids[1]. Therefore, self-aggregation of lipids is an enthalpy-driven process.

Geometrical structures of self-assembled lipids. Self-organized aggregates display a variety of structures, which differ in both topological and geometrical features (FIG. 5). The most common aggregates are micelles, spherical droplets of lipids in which the lipid heads point either outward (direct mesophases) or inward (inverse mesophases). In the case of direct

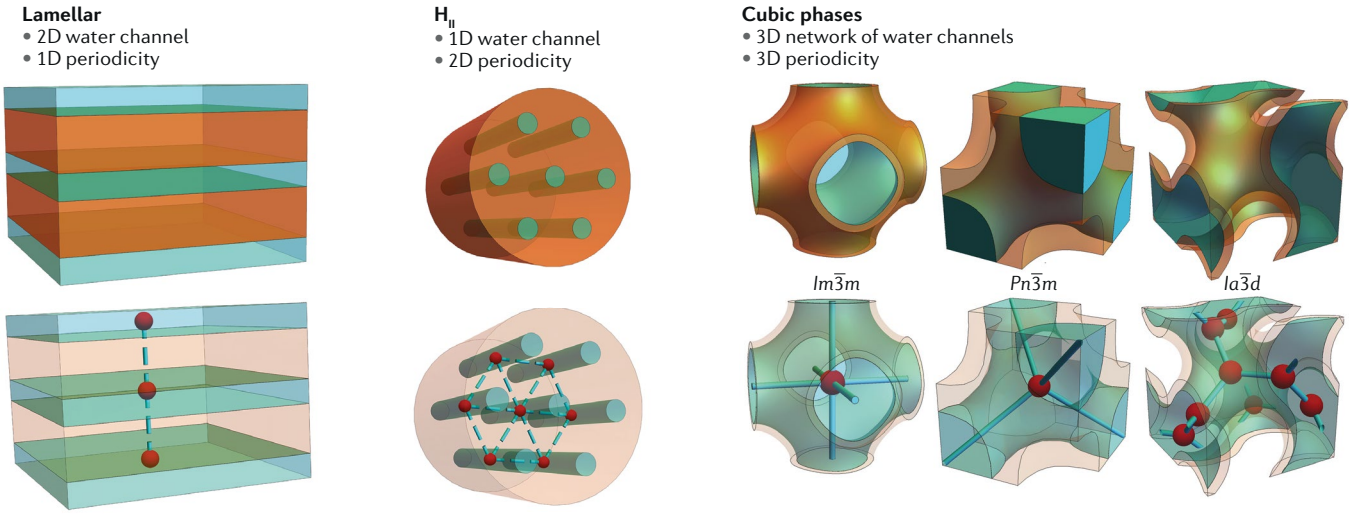

Fig. 5 | **Topological and geometrical features of some common inverse lipid mesophases.** The top images sketch the microscopic geometry of the mesophase (lipid-containing regions are depicted in orange; water regions are in cyan); the bottom images highlight the underlying topology, showing the periodic lattice identifying each structure. Dashed links between lattice nodes indicate that the corresponding water channels are not connected. The right-hand part is adapted from REF.[168], with the permission of AIP Publishing.

mesophases, these droplets are dispersed in water where they can be arranged on a lattice with cubic symmetry ($Fd\bar{3}m$). In the case of inverse mesophases, the water domains are confined within spheres. The spheres are organized in cubic-symmetric lattices ($Fd\bar{3}m$ or face-centred cubic) with the lipid tails spanning the continuous domains, with or without the presence of additional organic solvents or oil to reduce the lipid tail frustration. Another familiar geometry is the lamellar structure, in which lipids form flat bilayers intercalated by water slabs. Two subgroups are identified according to whether the lipid tails are amorphous (L_α) or crystalline (L_c). A less trivial case is provided by direct hexagonal phases (Hex), in which the lipids form micellar-like cylindrical aggregates ordered in a honeycomb lattice in the transverse direction. Inverse hexagonal phases (H_{II}) are like Hex but with reversed structural roles of lipids and water. Finally, the most intriguing geometries are provided by inverse bicontinuous cubic phases, in which a single lipid bilayer is arranged to form a minimal surface, characterized by zero mean curvature at each point, which encompasses the whole mesophase. This creates two physically separated yet identical sets of water channels with triple periodicity in space. The minimal surface followed by the lipid bilayer distinguishes between gyroid ($Ia\bar{3}d$ space group), diamond ($Pn\bar{3}m$) or primitive ($Im\bar{3}m$) structures, whose defining lattices are characterized by coordination numbers equal to 3, 4 and 6, respectively (FIG. 5).

H_{II} and cubic phases are possibly the most relevant geometries for foods, because they exist in excess water and are thus ideal hosts for delivery of drugs or nutraceuticals. Notably, these phases can either form macroscopic gel phases (bulk mesophases) or micro-sized dispersions (hexosomes and cubosomes). Apart from its topology, a mesophase is characterized by several geometrical features. The lattice parameter indicates the periodicity and usually lies in the range of single-digit nanometres to tens of nanometres; the radius of the corresponding nanochannels has values ranging from angstroms up to a few nanometres. By systematic experiments, the phase diagrams of several lipids (some of the most important in the field of food technology being monoolein, monolinolein and phytantriol[140–142]) have been constructed, detailing the features of aggregates as a function of temperature and water content.

Theory of lipid mesophases. There have been several attempts to understand the observed phase diagrams theoretically. The simplest and most widespread theory considers the critical packing parameter (CPP) = $v/(al)$, where v is the volume of the lipid tail, l is its length and a is the area of the lipid head[143]. When CPP ≈ 1, the lipid has a roughly cylindrical shape, and it is best accomodated in a lamellar geometry. For CPP > 1, the lipid tail occupies a larger volume than that accommodated by a cylindrical shape, thus inducing the formation of convex water domains. Consequently, inverse cubic phases and inverse hexagonal phases are favoured, with the latter preferred for larger CPP. Conversely, for CPP < 1 the volume spanned by the lipid tail is smaller than the corresponding cylinder, and direct phases are formed. The presence of hydrogen bonds with nearby water molecules induces a larger effective area of lipid heads[144]. Therefore, because heating the system disrupts hydrogen bonds, an increase of CPP upon temperature increase is expected, which explains the observed transitions from L_α to cubic to H_{II} phases. Nevertheless, this theory cannot predict the changes occurring when hydration is increased.

Self-consistent field theories provide further insights on the matter. A first theoretical attempt captured the details of the conformations adopted by the lipid tails[145], but the agreement with experimental results was not satisfactory, probably due to the simplistic representation of lipid heads as rigid bodies[139]. This issue was addressed in a subsequent model[144], in which lipid heads

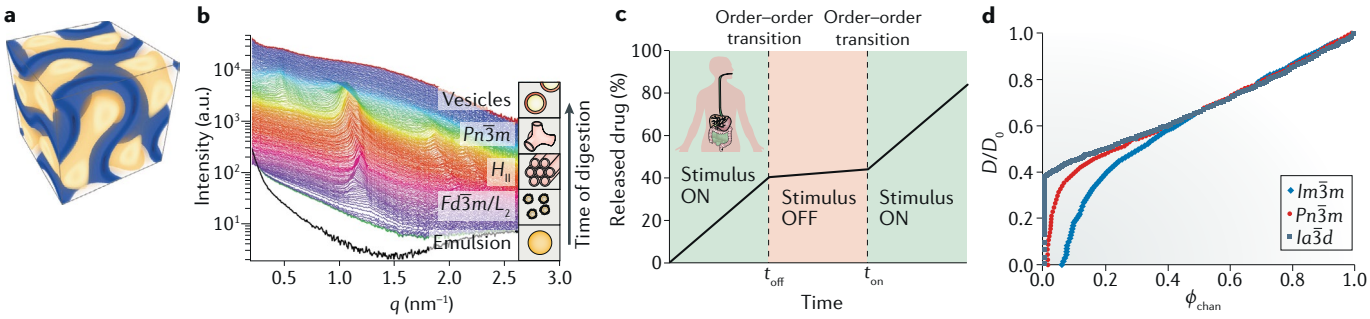

Fig. 6 | **Physics of lipid mesophases. a** | Electronic density map of a phytantriol-based mesophase with gyroid symmetry, supporting the validity of the parallel-surface model. **b** | Time evolution of mayonnaise microstructure under the action of lipase, as evidenced by profiles of SAXS (small-angle X-ray scattering) intensity versus magnitude of the scattering vector q. The inset images sketch the various structures displayed by the sample during the time of digestion. **c** | Controlled release achieved by tuning the topology and geometry of lipid mesophases via external stimuli. In this example, the stimulus is switched off at time t_{off} and then switched back on at time t_{on}. Example stimuli include temperature[167] as an exogenous stimulus or pH[155] as an endogenous stimulus. A pH-based stimulus is relevant for targeted delivery in chosen tracts of the digestive system (inset). **d** | Brownian dynamics simulations results for effective diffusion of water within different cubic phases. The effective diffusion coefficient D normalized by the bulk value D_0 is plotted against water content within a channel (ϕ_{chan}). For low water contents, D is dictated by geometry for mesophases at similar hydration. a.u, arbitrary units. Panel **a** is reproduced with permission from REF.[148], ACS. Panel **b** is reproduced with permission from REF.[137], ACS. Inset of panel **c** is reproduced with permission from REF.[155], ACS. Panel **d** is reproduced from REF.[168], with the permission of AIP Publishing.

could reversibly form hydrogen bonds with co-located water molecules. Apart from correctly reproducing the thermotropic transition $L_\alpha \rightarrow$ cubic $\rightarrow H_{II}$ upon heating, the theory also captured the transition from L_α to cubic obtained by increasing hydration. This provides a considerable step forward in the understanding of mesophase physics. However, it cannot reproduce the whole experimental phase diagram, which remains a challenge. For example, the model in REF.[144] predicts that the $Pn\bar{3}m$ cubic symmetry is only metastable, thus failing to account for its dominant presence in the experimental phase diagram of monoglycerides at high hydrations.

Another problem that has generated some debate relates to the geometrical details of the lipid–water interface. In particular, two alternatives have been proposed based on the incompatibility between constant mean curvature of the interface and constant thickness of the lipid bilayer. Assuming that the lipid–water interface has constant mean curvature provides a model that correctly captures the sequence of transitions that occur in the system upon increasing hydration[146]. Nevertheless, the stretching stress that this geometry introduces on the lipids has a high energetic cost, so a bilayer with constant thickness is instead expected to be favoured, corresponding to an interface parallel to the minimal surface[147]. The competition between these two models has been partially solved by an experiment on phytantriol-based mesophases, in which reconstructed electron density maps agreed with expectations from the parallel-surface model, in contrast to the constant mean curvature theory[148] (FIG. 6a). However, it is unclear whether this result is specific to phytantriol or can be generalized to other lipids, and further work focusing on different systems is needed to find a conclusive solution to the problem.

Characterization and control. It is clear from the previous section that theories provide general guidelines, but cannot yet be used to design de novo a system with targeted features in lipid self-assembly. This shortfall has been compensated by a large set of studies aimed at understanding how topology and geometry of lipid mesophases are affected by a number of factors[149]. Addition of co-surfactants usually results into swelling of both channels and lattice units, with a possible change of symmetry within the cubic family[150,151]. If the co-surfactant is charged, swelling can further be induced via electrostatic interactions[152,153] and controlled by adding salt[154] or tuning pH[155]. Other strategies include pressure control[156] or direct changes in the structure of the composing lipids via enzymatic digestion[157,158].

Apart from indicating how to control the properties of mesophases, these studies are also pivotal for understanding observations made for food systems. During digestion, the lipids in foods are subject to a change in pH from 1 in the stomach to 8 in the intestine, the action of enzymes and to the effects of bile salts[136]. The separate impact of lipase[159] and bile salts[160] has been addressed on model systems. Moreover, the evolution of the structural features of lipid aggregates within foods during intestinal digestion has been followed by using in vitro experiments mimicking the conditions in vivo. Detailed reports in the literature have been provided for mayonnaise[137], human milk[136] and bovine milk[135], as well as alterations induced by processing, such as homogenization or freeze-drying, that is, sublimation from a frozen water phase[161]. In all cases, it has been shown that increasing pH and digestion time monotonically drives the system towards more complex structures characterized by higher internal surface. Indeed, the sequence of mesophases isotropic fluid $\rightarrow Fd\bar{3}m \rightarrow H_{II} \rightarrow$ cubic is typically observed (FIG. 6b), in some cases together with a persistent lamellar phase[136]. This invariant result has been suggested as a possible mechanism in vivo for transporting poorly soluble molecules through the aqueous environment of the gut[135].

Molecular transport across lipid mesophases. The interest in understanding the transport of molecules in mesophases stems from the need to characterize mechanisms likely to act in vivo[135] and the possibility of manufacturing edible systems for delivery of nutraceuticals[162]. Moreover, mesophases have been proposed as nanoreactors for food reactions controlling aroma, taste or colour[163], whose yield is directly related to the diffusion properties of the reacting species. Importantly, incorporating micronutrients into lipid structures may affect the structure and function of the host mesophases[164].

Recent studies of molecular transport in lipid mesophases have addressed the impact of several features, such as the nature of diffusing molecules[165], the symmetry of the mesophase[164] and the hydration level[166]. In particular, transport in bicontinuous cubic phases is considerably faster than in H_{II}. This leads to the possibility of controlled triggering of the release behaviour of suitably produced mesophases (FIG. 6c). For instance, a combination of phytantriol and vitamin E acetate provided a mesophase with $Pn\bar{3}m$ symmetry at 30 °C and H_{II} at 40 °C (REF.[167]). This enables control of the molecular release by temperature, as fast release can be induced by cooling the system below physiological temperature. Heating leads to hampering of release. In another example, a pH-controlled switch has been obtained by combining monolinolein and linoleic acid, leading to slow diffusion at pH 2 and fast release at pH 7 (REF.[155]). Because these pH conditions are similar to those of stomach and intestine, the possibility has been opened of targeted molecular release in the intestinal tract (inset in FIG. 6c).

Differences in behaviour have also been reported among the various cubic symmetries. In particular, $Im\bar{3}m$ exhibits faster transport than $Pn\bar{3}m$. The two considered phases had different water content[151], but the role of symmetry was elucidated by Brownian dynamics simulations[168]. The simulations showed that if the water content is similar, then it is expected that transport is faster in $Pn\bar{3}m$ than in $Im\bar{3}m$ (FIG. 6d), thus ascribing the experimental observation to the greater hydration of the $Im\bar{3}m$ mesophase. Moreover, quantitative comparison between simulated and experimental diffusion coefficients has highlighted the role of water mobility, which shows very different features when compared with the bulk phase. In particular, the presence of hydrogen bonds with the lipid heads induces slow water self-diffusion in the three to four layers in proximity to the lipid bilayer[169]. Once the heterogeneity of water mobility observed in experiments was accounted for, simulation results showed quantitative agreement with the experimental data[168]. Further studies are needed before a complete understanding of molecular transport in lipid mesophases is achieved.

Perspectives

Despite the simplifications often introduced, the results from studies on polymers, colloids and surfactants provide tools to elucidate the properties of the primary constituents of foods, namely polysaccharides, proteins and lipids. However, in our Review, we have specifically tackled 'well-behaved' macronutrients and limited our discussion to situations where a single macronutrient interacts with water at thermodynamic equilibrium and with energies above the thermal fluctuation threshold ($E > k_BT$, FIG. 1b). In these cases, physical insight can be gained directly from equilibrium thermodynamics. However, foods are often found far from equilibrium[170]. For example, a colloidal dispersion of caseins, as found in skim milk, and a typical solution of a food polysaccharide such as xanthan, are both found individually at equilibrium, but when mixed they lead to a depletion-induced liquid–liquid phase separation which departs far from equilibrium binodal lines, instead following a non-equilibrium spinodal decomposition.

Even in such a complex non-equilibrium evolving food system, some universal features are preserved. For instance, for the casein–xanthan mixture, a universal signature has been reported for the structure factor which follows a master curve at any stage of the phase separation process — from the initial to the intermediate and transition regimes — when plotted against the scattering vector (inverse of the characteristic length) times the characteristic length of the dominant structural feature[171]. Perhaps even more surprisingly, some other universal features are maintained even in the final stage of the arrested spinodal decomposition, in which a gel is formed. These features include the scaling of the shear modulus of the gel with the timescale of structural arrest[172]. This illustrates that some of the universal laws originally developed for model colloidal systems can assist in the understanding of complex food systems even beyond equilibrium thermodynamics.

As a further note, there are still some soft matter tools that are underexploited in food contexts, such as force spectroscopy and polymer-based modelling of gel rheology, which could promote considerable advances in food science in the coming years.

The understanding of food systems based on physical concepts has made it possible to devise new applications that were unimaginable a decade ago. For example, protein self-assembly has been exploited in water purification[173] and in vivo iron integration[174]; lipid self-assembly has been suggested to improve bioavailability of vitamins in the bloodstream[175]. Complementary efforts from food scientists and soft condensed matter physicists are thus paramount to foster the development of new food technologies, which will provide unique opportunities to face the challenges of sustainable food production[176].

Published online 23 July 2019

1. Mezzenga, R., Schurtenberger, P., Burbidge, A. & Michel, M. Understanding foods as soft materials. *Nat. Mater.* **4**, 729–740 (2005).
2. Dominguez-Hernandez, E., Salaseviciene, A. & Ertbjerg, P. Low-temperature long-time cooking of meat: eating quality and underlying mechanisms. *Meat Sci.* **143**, 104–113 (2018).
3. McClements, D. J. Edible nanoemulsions: fabrication, properties, and functional performance. *Soft Matter* **7**, 2297–2316 (2011).
4. Lett, A. M., Yeomans, M. R., Norton, I. T. & Norton, J. E. Enhancing expected food intake behaviour, hedonics and sensory characteristics of oil-in-water emulsion systems through microstructural properties, oil droplet size and flavour. *Food Qual. Prefer.* **47**, 148–155 (2016).
5. Chiappisi, L. & Grillo, I. Looking into limoncello: the structure of the Italian liquor revealed by small-angle neutron scattering. *ACS Omega* **3**, 15407–15415 (2018).
6. Gallo, P. et al. Water: a tale of two liquids. *Chem. Rev.* **116**, 7463–7500 (2016).
7. Barnes, P., Finney, J. L., Nicholas, J. D. & Quinn, J. E. Cooperative effects in simulated water. *Nature* **282**, 459–464 (1979).
8. Luzar, A. & Chandler, D. Hydrogen-bond kinetics in liquid water. *Nature* **379**, 55–57 (1996).
9. Poole, P. H., Sciortino, F., Essmann, U. & Stanley, H. E. Phase behaviour of metastable water. *Nature* **360**, 324–328 (1992).

10. Palmer, J. C., Poole, P. H., Sciortino, F. & Debenedetti, P. G. Advances in computational studies of the liquid–liquid transition in water and water-like models. *Chem. Rev.* **118**, 9129–9151 (2018).
11. Urbic, T. & Dill, K. A. Water is a cagey liquid. *J. Am. Chem. Soc*, https://doi.org/10.1021/jacs.8b08856 (2018).
12. Nomura, K. et al. Evidence of low-density and high-density liquid phases and isochore end point for water confined to carbon nanotube. *Proc. Natl Acad. Sci. USA* **114**, 4066–4071 (2017).
13. Israelachvili, J. N. *Intermolecular and Surface Forces*, 3rd edn (Academic, 2011).
14. de Gennes, P.-G. *Scaling Concepts in Polymer physics* (Cornell Univ. Press, 1979)..
15. Stevens, M. J., Berezney, J. P. & Saleh, O. A. The effect of chain stiffness and salt on the elastic response of a polyelectrolyte. *J. Chem. Phys.* **149**, 163328 (2018).
16. Berezney, J. P. & Saleh, O. A. Electrostatic effects on the conformation and elasticity of hyaluronic acid, a moderately flexible polyelectrolyte. *Macromolecules* **50**, 1085–1089 (2017).
17. Sassi, A. S., Assenza, S. & De Los Rios, P. Shape of a stretched polymer. *Phys. Rev. Lett.* **119**, 037801 (2017).
18. Rubinstein, M. & Colby, R. H. *Polymer Physics* (Oxford Univ. Press, 2003).
19. Jung, J. M., Savin, G., Pouzot, M., Schmitt, C. & Mezzenga, R. Structure of heat-induced beta-lactoglobulin aggregates and their complexes with sodium-dodecyl sulfate. *Biomacromolecules* **9**, 2477–2486 (2008).
20. Ortiz-Tafoya, M. C., Rolland-Sabate, A., Garnier, C., Valadez-Garcia, J. & Tecante, A. Thermal, conformational and rheological properties of kappa-carrageenan-sodium stearoyl lactylate gels and solutions. *Carbohydr. Polym.* **193**, 289–297 (2018).
21. Hofmann, H. et al. Polymer scaling laws of unfolded and intrinsically disordered proteins quantified with single-molecule spectroscopy. *Proc. Natl Acad. Sci. USA* **109**, 16155–16160 (2012).
22. Kellner, R. et al. Single-molecule spectroscopy reveals chaperone-mediated expansion of substrate protein. *Proc. Natl Acad. Sci. USA* **111**, 13355–13360 (2014).
23. Clisby, N. Accurate estimate of the critical exponent nu for self-avoiding walks via a fast implementation of the pivot algorithm. *Phys. Rev. Lett.* **104**, 055702 (2010).
24. Le Guillou, J. C. & Zinn-Justin, J. Critical exponents from field theory. *Phys. Rev. B* **21**, 3976–3998 (1980).
25. Kohn, J. E. et al. Random-coil behavior and the dimensions of chemically unfolded proteins. *Proc. Natl Acad. Sci. USA* **101**, 12491–12496 (2004).
26. Valle, F., Favre, M., De Los Rios, P., Rosa, A. & Dietler, G. Scaling exponents and probability distributions of DNA end-to-end distance. *Phys. Rev. Lett.* **95**, 158105 (2005).
27. Dahesh, M., Banc, A., Duri, A., Morel, M. H. & Ramos, L. Polymeric assembly of gluten proteins in an aqueous ethanol solvent. *J. Phys. Chem. B* **118**, 11065–11076 (2014).
28. Dalheim, M. O., Arnfinnsdottir, N. B., Widmalm, G. & Christensen, B. E. The size and shape of three water-soluble, non-ionic polysaccharides produced by lactic acid bacteria: a comparative study. *Carbohydr. Polym.* **142**, 91–97 (2016).
29. Lara, C., Usov, I., Adamcik, J. & Mezzenga, R. Sub-persistence-length complex scaling behavior in lysozyme amyloid fibrils. *Phys. Rev. Lett.* **107**, 238101 (2011).
30. Usov, I., Adamcik, J. & Mezzenga, R. Polymorphism complexity and handedness inversion in serum albumin amyloid fibrils. *ACS Nano* **7**, 10465–10474 (2013).
31. Schuler, B., Soranno, A., Hofmann, H. & Nettels, D. Single-molecule FRET spectroscopy and the polymer physics of unfolded and intrinsically disordered proteins. *Annu. Rev. Biophys.* **45**, 207–231 (2016).
32. Gittes, F., Mickey, B., Nettleton, J. & Howard, J. Flexural rigidity of microtubules and actin filaments measured from thermal fluctuations in shape. *J. Cell Biol.* **120**, 923–934 (1993).
33. Adamcik, J. et al. Understanding amyloid aggregation by statistical analysis of atomic force microscopy images. *Nat. Nanotechnol.* **5**, 423–428 (2010).
34. Loveday, S. M. & Gunning, A. P. Nanomechanics of pectin-linked beta-lactoglobulin nanofibril bundles. *Biomacromolecules* **19**, 2834–2840 (2018).
35. Teckentrup, J. et al. Comparative analysis of different xanthan samples by atomic force microscopy. *J. Biotechnol.* **257**, 2–8 (2017).
36. Jiang, X., Ryoki, A. & Terao, K. Dimensional and hydrodynamic properties of cellulose tris (alkylcarbamate)s in solution: side chain dependent conformation in tetrahydrofuran. *Polymer* **112**, 152–158 (2017).
37. Ryoki, A., Kim, D., Kitamura, S. & Terao, K. Linear and cyclic amylose derivatives having brush like side groups in solution: amylose tris(n-octadecylcarbamate) s. *Polymer* **137**, 13–21 (2018).
38. Terao, K. et al. Side-chain-dependent helical conformation of amylose alkylcarbamates: amylose tris(ethylcarbamate) and amylose tris(n-hexylcarbamate). *J. Phys. Chem. B* **116**, 12714–12720 (2012).
39. Sano, Y. et al. Solution properties of amylose tris (n-butylcarbamate). Helical and global conformation in alcohols. *Polymer* **51**, 4243–4248 (2010).
40. Schefer, L., Usov, I. & Mezzenga, R. Anomalous stiffening and ion-induced coil–helix transition of carrageenans under monovalent salt conditions. *Biomacromolecules* **16**, 985–991 (2015).
41. Schefer, L., Adamcik, J. & Mezzenga, R. Unravelling secondary structure changes on individual anionic polysaccharide chains by atomic force microscopy. *Angew. Chem.* **53**, 5376–5379 (2014).
42. Tirrell, M. V., Granick, S. & Muthukumar, M. Preface: special topic on chemical physics of charged macromolecules. *J. Chem. Phys.* **149**, 163001 (2018).
43. Odijk, T. Polyelectrolytes near the rod limit. *J. Polym. Sci. Polym. Phys. Ed.* **15**, 477–483 (1977).
44. Skolnick, J. & Fixman, M. Electrostatic persistence length of a wormlike polyelectrolyte. *Macromolecules* **10**, 944–948 (1977).
45. Barrat, J. L. & Joanny, J. F. Persistence length of polyelectrolyte chains. *Europhys. Lett.* **24**, 333–338 (1993).
46. Caliskan, G. et al. Persistence length changes dramatically as RNA folds. *Phys. Rev. Lett.* **95**, 268303 (2005).
47. Savelyev, A. Do monovalent mobile ions affect DNA's flexibility at high salt content? *Phys. Chem. Chem. Phys.* **14**, 2250–2254 (2012).
48. Saleh, O. A., McIntosh, D. B., Pincus, P. & Ribeck, N. Nonlinear low-force elasticity of single-stranded DNA molecules. *Phys. Rev. Lett.* **102**, 068301 (2009).
49. Sim, A. Y., Lipfert, J., Herschlag, D. & Doniach, S. Salt dependence of the radius of gyration and flexibility of single-stranded DNA in solution probed by small-angle x-ray scattering. *Phys. Rev. E* **86**, 021901 (2012).
50. Micka, U. & Kremer, K. Persistence length of the Debye–Hückel model of weakly charged flexible polyelectrolyte chains. *Phys. Rev. E* **54**, 2653–2662 (1996).
51. Manning, G. S. Limiting laws and counterion condensation in polyelectrolyte solutions. I. Colligative properties. *J. Chem. Phys.* **51**, 924–933 (1969).
52. Dobrynin, A. & Rubinstein, M. Theory of polyelectrolytes in solutions and at surfaces. *Prog. Polym. Sci.* **30**, 1049–1118 (2005).
53. Irani, A. H., Owen, J. L., Mercadante, D. & Williams, M. A. Molecular dynamics simulations illuminate the role of counterion condensation in the electrophoretic transport of homogalacturonans. *Biomacromolecules* **18**, 505–516 (2017).
54. Netz, R. R. & Orland, H. Variational charge renormalization in charged systems. *Eur. Phys. J. E* **11**, 301–311 (2003).
55. Marko, J. F. & Siggia, E. D. Stretching DNA. *Macromolecules* **28**, 8759–8770 (1995).
56. Bustamante, C., Bryant, Z. & Smith, S. B. Ten years of tension: single-molecule DNA mechanics. *Nature* **421**, 423–427 (2003).
57. Rief, M., Gautel, M., Oesterhelt, F., Fernandez, J. M. & Gaub, H. E. Reversible unfolding of individual titin immunoglobulin domains by AFM. *Science* **276**, 1109–1112 (1997).
58. Rief, M., Oesterhelt, F., Heymann, B. & Gaub, H. E. Single molecule force spectroscopy on polysaccharides by atomic force microscopy. *Science* **275**, 1295–1297 (1997).
59. Camunas-Soler, J., Ribezzi-Crivellari, M. & Ritort, F. Elastic properties of nucleic acids by single-molecule force spectroscopy. *Annu. Rev. Biophys.* **45**, 65–84 (2016).
60. Hughes, M. L. & Dougan, L. The physics of pulling polyproteins: a review of single molecule force spectroscopy using the AFM to study protein unfolding. *Rep. Prog. Phys. Phys. Soc.* **79**, 076601 (2016).
61. Lakshminarayanan, A., Richard, M. & Davis, B. G. Studying glycobiology at the single-molecule level. *Nat. Rev. Chem.* **2**, 148–159 (2018).
62. Naranjo, T. et al. Dynamics of individual molecular shuttles under mechanical force. *Nat. Commun.* **9**, 4512 (2018).
63. Camunas-Soler, J., Alemany, A. & Ritort, F. Experimental measurement of binding energy, selectivity, and allostery using fluctuation theorems. *Science* **355**, 412–415 (2017).
64. Gunning, A. P. & Morris, V. J. Getting the feel of food structure with atomic force microscopy. *Food Hydrocoll.* **78**, 62–76 (2018).
65. Qian, L., Bao, Y., Duan, W. & Cui, S. Effects of water content of the mixed solvent on the single-molecule mechanics of amylose. *ACS Macro Lett.* **7**, 672–676 (2018).
66. Marszalek, P. E., Li, H., Oberhauser, A. F. & Fernandez, J. M. Chair–boat transitions in single polysaccharide molecules observed with force-ramp AFM. *Proc. Natl Acad. Sci. USA* **99**, 4278–4283 (2002).
67. Marszalek, P. E., Oberhauser, A. F., Pang, Y. P. & Fernandez, J. M. Polysaccharide elasticity governed by chair–boat transitions of the glucopyranose ring. *Nature* **396**, 661–664 (1998).
68. Lara, Cc, Adamcik, J., Jordens, S. & Mezzenga, R. General self-assembly mechanism converting hydrolyzed globular proteins into giant multistranded amyloid ribbons. *Biomacromolecules* **12**, 1868–1875 (2011).
69. Assenza, S., Adamcik, J., Mezzenga, R. & De Los Rios, P. Universal behavior in the mesoscale properties of amyloid fibrils. *Phys. Rev. Lett.* **113**, 268103 (2014).
70. Goldsbury, C. S. et al. Polymorphic fibrillar assembly of human amylin. *J. Struct. Biol.* **119**, 17–27 (1997).
71. Moffat, J., Morris, V. J., Al-Assaf, S. & Gunning, A. P. Visualisation of xanthan conformation by atomic force microscopy. *Carbohydr. Polym.* **148**, 380–389 (2016).
72. Koziol, A., Cybulska, J., Pieczywek, P. M. & Zdunek, A. Evaluation of structure and assembly of xyloglucan from tamarind seed (*Tamarindus indica* L.) with atomic force microscopy. *Food Biophys.* **10**, 396–402 (2015).
73. Xiao, M. et al. Investigation on curdlan dissociation by heating in water. *Food Hydrocoll.* **70**, 57–64 (2017).
74. Schefer, L., Adamcik, J., Diener, M. & Mezzenga, R. Supramolecular chiral self-assembly and supercoiling behavior of carrageenans at varying salt conditions. *Nanoscale* **7**, 16182–16188 (2015).
75. Mezzenga, R. & Fischer, P. The self-assembly, aggregation and phase transitions of food protein systems in one, two and three dimensions. *Rep. Prog. Phys. Phys. Soc.* **76**, 046601 (2013).
76. Fusco, D. & Charbonneau, P. Soft matter perspective on protein crystal assembly. *Colloids Surf. B* **137**, 22–31 (2016).
77. Platten, F., Valadez-Perez, N. E., Castaneda-Priego, R. & Egelhaaf, S. U. Extended law of corresponding states for protein solutions. *J. Chem. Phys.* **142**, 174905 (2015).
78. Platten, F., Hansen, J., Wagner, D. & Egelhaaf, S. U. Second virial coefficient as determined from protein phase behavior. *J. Phys. Chem. Lett.* **7**, 4008–4014 (2016).
79. Baxter, R. J. Percus–yevick equation for hard spheres with surface adhesion. *J. Chem. Phys.* **49**, 2770–2774 (1968).
80. Asakura, S. & Oosawa, F. Interaction between particles suspended in solutions of macromolecules. *J. Polym. Sci.* **33**, 183–192 (1958).
81. Asakura, S. & Oosawa, F. On Interaction between two bodies immersed in a solution of macromolecules. *J. Chem. Phys.* **22**, 1255–1256 (1954).
82. Woldeyes, M. A., Calero-Rubio, C., Furst, E. M. & Roberts, C. J. Predicting protein interactions of concentrated globular protein solutions using colloidal models. *J. Phys. Chem. B* **121**, 4756–4767 (2017).
83. Braun, M. K. et al. Strong isotope effects on effective interactions and phase behavior in protein solutions in the presence of multivalent ions. *J. Phys. Chem. B* **121**, 1731–1739 (2017).
84. Bucciarelli, S. et al. Extended law of corresponding states applied to solvent isotope effect on a globular protein. *J. Phys. Chem. Lett.* **7**, 1610–1615 (2016).
85. Hansen, J., Platten, F., Wagner, D. & Egelhaaf, S. U. Tuning protein–protein interactions using cosolvents: specific effects of ionic and non-ionic additives on protein phase behavior. *Phys. Chem. Chem. Phys.* **18**, 10270–10280 (2016).
86. Noro, M. G. & Frenkel, D. Extended corresponding-states behavior for particles with variable range attractions. *J. Chem. Phys.* **113**, 2941–2944 (2000).

87. Bárcenas, M., Castellanos, V., Reyes, Y., Odriozola, G. & Orea, P. Phase behaviour of short range triangle well fluids: a comparison with lysozyme suspensions. *J. Mol. Liq.* **225**, 723–729 (2017).
88. Sciortino, F. & Zaccarelli, E. Reversible gels of patchy particles. *Curr. Opin. Solid State Mater. Sci.* **15**, 246–253 (2011).
89. Liu, H., Kumar, S. K. & Sciortino, F. Vapor-liquid coexistence of patchy models: relevance to protein phase behavior. *J. Chem. Phys.* **127**, 084902 (2007).
90. Gogelein, C. et al. A simple patchy colloid model for the phase behavior of lysozyme dispersions. *J. Chem. Phys.* **129**, 085102 (2008).
91. Foffi, G. & Sciortino, F. On the possibility of extending the Noro–Frenkel generalized law of correspondent states to nonisotropic patchy interactions. *J. Phys. Chem. B* **111**, 9702–9705 (2007).
92. Boire, A., Sanchez, C., Morel, M. H., Lettinga, M. P. & Menut, P. Dynamics of liquid–liquid phase separation of wheat gliadins. *Sci. Rep.* **8**, 14441 (2018).
93. Grimaldo, M. et al. Salt-induced universal slowing down of the short-time self-diffusion of a globular protein in aqueous solution. *J. Phys. Chem. Lett.* **6**, 2577–2582 (2015).
94. Bucciarelli, S. et al. Dramatic influence of patchy attractions on short-time protein diffusion under crowded conditions. *Sci. Adv.* **2**, e1601432 (2016).
95. Cai, J. & Sweeney, A. M. The proof is in the pidan: generalizing proteins as patchy particles. *ACS Cent. Sci.* **4**, 840–853 (2018).
96. Cai, J., Townsend, J. P., Dodson, T. C., Heiney, P. A. & Sweeney, A. M. Eye patches: protein assembly of index-gradient squid lenses. *Science* **357**, 564–569 (2017).
97. Fries, M. R. et al. Multivalent-ion-activated protein adsorption reflecting bulk reentrant behavior. *Phys. Rev. Lett.* **119**, 228001 (2017).
98. Roosen-Runge, F., Zhang, F., Schreiber, F. & Roth, R. Ion-activated attractive patches as a mechanism for controlled protein interactions. *Sci. Rep.* **4**, 7016 (2014).
99. Stopper, D., Hirschmann, F., Oettel, M. & Roth, R. Bulk structural information from density functionals for patchy particles. *J. Chem. Phys.* **149**, 224503 (2018).
100. Yigit, C., Heyda, J. & Dzubiella, J. Charged patchy particle models in explicit salt: ion distributions, electrostatic potentials, and effective interactions. *J. Chem. Phys.* **143**, 064904 (2015).
101. Blanco, M. A. & Shen, V. K. Effect of the surface charge distribution on the fluid phase behavior of charged colloids and proteins. *J. Chem. Phys.* **145**, 155102 (2016).
102. Garcia, N. A., Gnan, N. & Zaccarelli, E. Effective potentials induced by self-assembly of patchy particles. *Soft Matter* **13**, 6051–6058 (2017).
103. Newton, A. C., Kools, R., Swenson, D. W. H. & Bolhuis, P. G. The opposing effects of isotropic and anisotropic attraction on association kinetics of proteins and colloids. *J. Chem. Phys.* **147**, 155101 (2017).
104. Bleibel, J. et al. Two time scales for self and collective diffusion near the critical point in a simple patchy model for proteins with floating bonds. *Soft Matter* **14**, 8006–8016 (2018).
105. Jansens, K. J. A. et al. Rational design of amyloid-like fibrillary structures for tailoring food protein techno-functionality and their potential health implications. *Compr. Rev. Food Sci. Food Saf.* **18**, 84–105 (2019).
106. Boire, A. et al. Soft matter approaches for controlling food protein interactions and assembly. *Annu. Rev. Food Sci. Technol*. https://doi.org/10.1146/annurev-food-032818-121907 (2019).
107. McManus, J. J., Charbonneau, P., Zaccarelli, E. & Asherie, N. The physics of protein self-assembly. *Curr. Opin. Colloid Interface Sci.* **22**, 73–79 (2016).
108. Sciortino, F., Mossa, S., Zaccarelli, E. & Tartaglia, P. Equilibrium cluster phases and low-density arrested disordered states: the role of short-range attraction and long-range repulsion. *Phys. Rev. Lett.* **93**, 055701 (2004).
109. Stradner, A. et al. Equilibrium cluster formation in concentrated protein solutions and colloids. *Nature* **432**, 492–495 (2004).
110. Jachimska, B., Wasilewska, M. & Adamczyk, Z. Characterization of globular protein solutions by dynamic light scattering, electrophoretic mobility, and viscosity measurements. *Langmuir* **24**, 6866–6872 (2008).
111. Ianeselli, L. et al. Protein-protein interactions in ovalbumin solutions studied by small-angle scattering: effect of ionic strength and the chemical nature of cations. *J. Phys. Chem. B* **114**, 3776–3783 (2010).
112. Shukla, A. et al. Absence of equilibrium cluster phase in concentrated lysozyme solutions. *Proc. Natl Acad. Sci. USA* **105**, 5075–5080 (2008).
113. Liu, Y., Fratini, E., Baglioni, P., Chen, W. R. & Chen, S. H. Effective long-range attraction between protein molecules in solutions studied by small angle neutron scattering. *Phys. Rev. Lett.* **95**, 118102 (2005).
114. StradnerA.., Cardinaux FEgelhaaf, S. U. & Schurtenberger, P. Do equilibrium clusters exist in concentrated lysozyme solutions? *Proc. Natl Acad. Sci. USA* **105**, E75; author reply E76, https://doi.org/10.1073/pnas.0805815105 (2008).
115. Cardinaux, F. et al. Cluster-driven dynamical arrest in concentrated lysozyme solutions. *J. Phys. Chem. B* **115**, 7227–7237 (2011).
116. Bergman, M. J., Garting, T., Schurtenberger, P. & Stradner, A. Experimental evidence for a cluster glass transition in concentrated lysozyme solutions. *J. Phys. Chem. B* **123**, 2432–2438 (2019).
117. Riest, J., Nagele, G., Liu, Y., Wagner, N. J. & Godfrin, P. D. Short-time dynamics of lysozyme solutions with competing short-range attraction and long-range repulsion: experiment and theory. *J. Chem. Phys.* **148**, 065101 (2018).
118. Kundu, S., Aswal, V. K. & Kohlbrecher, J. Synergistic effect of temperature, protein and salt concentration on structures and interactions among lysozyme proteins. *Chem. Phys. Lett.* **657**, 90–94 (2016).
119. Skar-Gislinge, N. et al. A colloid approach to self-assembling antibodies. *Preprint at* https://arxiv.org/abs/1810.01160 (2018).
120. Vega, C. & Mercadé-Prieto, R. Culinary biophysics: on the nature of the 6X°C egg. *Food Biophys.* **6**, 152–159 (2011).
121. Lepetit, J. A theoretical approach of the relationships between collagen content, collagen cross-links and meat tenderness. *Meat Sci.* **76**, 147–159 (2007).
122. Miocinovic, J. et al. Rheological and textural properties of goat and cow milk set type yoghurts. *Int. Dairy J.* **58**, 43–45 (2016).
123. Baussay, K., Bon, C. L., Nicolai, T., Durand, D. & Busnel, J.-P. Influence of the ionic strength on the heat-induced aggregation of the globular protein β-lactoglobulin at pH 7. *Int. J. Biol. Macromol.* **34**, 21–28 (2004).
124. Pouzot, M., Nicolai, T., Durand, D. & Benyahia, L. Structure factor and elasticity of a heat-set globular protein gel. *Macromolecules* **37**, 614–620 (2004).
125. Nieuwland, M., Bouwman, W. G., Pouvreau, L., Martin, A. H. & de Jongh, H. H. J. Relating water holding of ovalbumin gels to aggregate structure. *Food Hydrocoll.* **52**, 87–94 (2016).
126. Chen, N., Zhao, M., Chassenieux, C. & Nicolai, T. Structure of self-assembled native soy globulin in aqueous solution as a function of the concentration and the pH. *Food Hydrocoll.* **56**, 417–424 (2016).
127. Banc, A. et al. Small angle neutron scattering contrast variation reveals heterogeneities of interactions in protein gels. *Soft Matter* **12**, 5340–5352 (2016).
128. Dahesh, M., Banc, A., Duri, A., Morel, M.-H. & Ramos, L. Spontaneous gelation of wheat gluten proteins in a food grade solvent. *Food Hydrocoll.* **52**, 1–10 (2016).
129. Ahmed, K. F., Aschi, A. & Nicolai, T. Formation and characterization of chitosan–protein particles with fractal whey protein aggregates. *Colloids Surf. B* **169**, 257–264 (2018).
130. Doi, M. & Onuki, A. Dynamic coupling between stress and composition in polymer solutions and blends. *J. Phys. II* **2**, 1631–1656 (1992).
131. Kantor, Y. & Webman, I. Elastic properties of random percolating systems. *Phys. Rev. Lett.* **52**, 1891–1894 (1984).
132. Rafe, A. & Razavi, S. M. A. Scaling law, fractal analysis and rheological characteristics of physical gels cross-linked with sodium trimetaphosphate. *Food Hydrocoll.* **62**, 58–65 (2017).
133. MacKintosh, F. C., Kas, J. & Janmey, P. A. Elasticity of semiflexible biopolymer networks. *Phys. Rev. Lett.* **75**, 4425–4428 (1995).
134. Cao, Y., Bolisetty, S., Adamcik, J. & Mezzenga, R. Elasticity in physically cross-linked amyloid fibril networks. *Phys. Rev. Lett.* **120**, 158103 (2018).
135. Salentinig, S., Phan, S., Khan, J., Hawley, A. & Boyd, B. J. Formation of highly organized nanostructures during the digestion of milk. *ACS nano* **7**, 10904–10911 (2013).
136. Salentinig, S., Phan, S., Hawley, A. & Boyd, B. J. Self-assembly structure formation during the digestion of human breast milk. *Angew. Chem.* **54**, 1600–1603 (2015).
137. Salentinig, S., Amenitsch, H. & Yaghmur, A. In situ monitoring of nanostructure formation during the digestion of mayonnaise. *ACS omega* **2**, 1441–1446 (2017).
138. Leibler, L. Theory of microphase separation in block copolymers. *Macromolecules* **13**, 1602–1617 (1980).
139. Mezzenga, R. Physics of self-assembly of lyotropic liquid crystals. https://doi.org/10.1002/9781118336632.ch1 (2012).
140. Qiu, H. & Caffrey, M. The phase diagram of the monoolein/water system: metastability and equilibrium aspects. *Biomaterials* **21**, 223–234 (2000).
141. Mezzenga, R. et al. Shear rheology of lyotropic liquid crystals: a case study. *Langmuir* **21**, 3322–3333 (2005).
142. Barauskas, J. & Landh, T. Phase Behavior of the phytantriol/water system. *Langmuir* **19**, 9562–9565 (2003).
143. Israelachvili, J. N., Mitchell, D. J. & Ninham, B. W. Theory of self-assembly of hydrocarbon amphiphiles into micelles and bilayers. *J. Chem. Soc. Faraday Trans. 2* **72**, 1525 (1976).
144. Lee, W. B., Mezzenga, R. & Fredrickson, G. H. Anomalous phase sequences in lyotropic liquid crystals. *Phys. Rev. Lett.* **99**, 187801 (2007).
145. Müller, M. & Schick, M. Calculation of the phase behavior of lipids. *Phys. Rev. E* **57**, 6973–6978 (1998).
146. Templer, R. H., Seddon, J. M., Duesing, P. M., Winter, R. & Erbes, J. Modeling the phase behavior of the inverse hexagonal and inverse bicontinuous cubic phases in 2:1 fatty acid/phosphatidylcholine mixtures. *J. Phys. Chem. B* **102**, 7262–7271 (1998).
147. Schwarz, U. S. & Gompper, G. Bending frustration of lipid–water mesophases based on cubic minimal surfaces. *Langmuir* **17**, 2084–2096 (2001).
148. Oka, T., Ohta, N. & Hyde, S. Polar–nonpolar interfaces of inverse bicontinuous cubic phases in phytantriol/water system are parallel to triply periodic minimal surfaces. *Langmuir* **34**, 15462–15469 (2018).
149. Barriga, H. M. G., Holme, M. N. & Stevens, M. M. Cubosomes: the next generation of smart lipid nanoparticles? *Angew. Chem*. https://doi.org/10.1002/anie.201804067 (2018).
150. Yaghmur, A., de Campo, L., Sagalowicz, L., Leser, M. E. & Glatter, O. Control of the internal structure of MLO-based isasomes by the addition of diglycerol monooleate and soybean phosphatidylcholine. *Langmuir* **22**, 9919–9927 (2006).
151. Negrini, R. & Mezzenga, R. Diffusion, molecular separation, and drug delivery from lipid mesophases with tunable water channels. *Langmuir* **28**, 16455–16462 (2012).
152. Tyler, A. I. et al. Electrostatic swelling of bicontinuous cubic lipid phases. *Soft Matter* **11**, 3279–3286 (2015).
153. Leung, S. S. W. & Leal, C. The stabilization of primitive bicontinuous cubic phases with tunable swelling over a wide composition range. *Soft Matter*. https://doi.org/10.1039/c8sm02059k (2018).
154. Brasnett, C., Longstaff, G., Compton, L. & Seddon, A. Effects of cations on the behaviour of lipid cubic phases. *Sci. Rep.* **7**, 8229 (2017).
155. Negrini, R. & Mezzenga, R. pH-responsive lyotropic liquid crystals for controlled drug delivery. *Langmuir* **27**, 5296–5303 (2011).
156. Barriga, H. M. et al. Temperature and pressure tuneable swollen bicontinuous cubic phases approaching nature's length scales. *Soft Matter* **11**, 600–607 (2015).
157. Fong, W.-K. et al. Dynamic formation of nanostructured particles from vesicles via invertase hydrolysis for on-demand delivery. *RSC Adv.* **7**, 4368–4377 (2017).
158. Fong, W. K. et al. Generation of geometrically ordered lipid-based liquid-crystalline nanoparticles using biologically relevant enzymatic processing. *Langmuir* **30**, 5373–5377 (2014).
159. Salentinig, S., Sagalowicz, L., Leser, M. E., Tedeschi, C. & Glatter, O. Transitions in the internal structure of lipid droplets during fat digestion. *Soft Matter* **7**, 650–661 (2011).
160. Sadeghpour, A., Rappolt, M., Misra, S. & Kulkarni, C. V. Bile salts caught in the act: from emulsification to nanostructural reorganization of lipid self-assemblies. *Langmuir* **34**, 13626–13637 (2018).
161. Clulow, A. J., Salim, M., Hawley, A. & Boyd, B. J. A closer look at the behaviour of milk lipids during digestion. *Chem. Phys. lipids* **211**, 107–116 (2018).
162. McClements, D. J. Encapsulation, protection, and release of hydrophilic active components: potential and limitations of colloidal delivery systems. *Adv. Colloid Interface Sci.* **219**, 27–53 (2015).
163. Sagalowicz, L. et al. Lipid self-assembled structures for reactivity control in food. *Phil. Trans. A* **374**, https://doi.org/10.1098/rsta.2015.0136 (2016).

164. Martiel, I. et al. Oil and drug control the release rate from lyotropic liquid crystals. *J. Control. Release* **204**, 78–84 (2015).
165. Clogston, J. & Caffrey, M. Controlling release from the lipidic cubic phase. Amino acids, peptides, proteins and nucleic acids. *J. Control. Release* **107**, 97–111 (2005).
166. Meikle, T. G. et al. Predicting the release profile of small molecules from within the ordered nanostructured lipidic bicontinuous cubic phase using translational diffusion coefficients determined by PFG-NMR. *Nanoscale* **9**, 2471–2478 (2017).
167. Fong, W. K., Hanley, T. & Boyd, B. J. Stimuli responsive liquid crystals provide 'on-demand' drug delivery in vitro and in vivo. *J. Control. Release* **135**, 218–226 (2009).
168. Assenza, S. & Mezzenga, R. Curvature and bottlenecks control molecular transport in inverse bicontinuous cubic phases. *J. Chem. Phys.* **148**, 054902 (2018).
169. Kim, J. et al. Ultrafast hydration dynamics in the lipidic cubic phase: discrete water structures in nanochannels. *J. Phys. Chem. B* **110**, 21994–22000 (2006).
170. Mezzenga, R. Equilibrium and non-equilibrium structures in complex food systems. *Food Hydrocoll.* **21**, 674–682 (2007).
171. Bhat, S., Tuinier, R. & Schurtenberger, P. Spinodal decomposition in a food colloid–biopolymer mixture: evidence for a linear regime. *J. Phys. Condens Matter* **18**, L339–L346 (2006).
172. Mahmoudi, N. & Stradner, A. Structural arrest and dynamic localization in biocolloidal gels. *Soft Matter* **13**, 4629–4635 (2017).
173. Bolisetty, S. & Mezzenga, R. Amyloid-carbon hybrid membranes for universal water purification. *Nat. Nanotechnol.* **11**, 365–371 (2016).
174. Shen, Y. et al. Amyloid fibril systems reduce, stabilize and deliver bioavailable nanosized iron. *Nat. Nanotechnol.* **12**, 642–647 (2017).
175. Nagy, K. et al. Vitamin E and vitamin E acetate absorption from self-assembly systems under pancreas insufficiency conditions. *Chimia* **68**, 129–134 (2014).
176. Springmann, M. et al. Options for keeping the food system within environmental limits. *Nature* **562**, 519–525 (2018).
177. Matsuyama, A. & Tanaka, F. Theory of solvation-induced reentrant phase separation in polymer solutions. *Phys. Rev. Lett.* **65**, 341–344 (1990).
178. Takahashi, M., Shimazaki, M. & Yamamoto, J. Thermoreversible gelation and phase separation in aqueous methyl cellulose solutions. *J. Polym. Sci. B* **39**, 91–100 (2001).
179. Rwei, S.-P. & Lyu, M.-S. 3-D phase diagram of HPC/H_2O/H_3PO_4 tertiary system. *Cellulose* **19**, 1065–1074 (2012).
180. Brangwynne, C. P., Tompa, P. & Pappu, R. V. Polymer physics of intracellular phase transitions. *Nat. Phys.* **11**, 899–904 (2015).
181. Pak, C. W. et al. Sequence determinants of intracellular phase separation by complex coacervation of a disordered protein. *Mol. Cell* **63**, 72–85 (2016).
182. Wu, X. et al. Gelation of β-lactoglobulin and its fibrils in the presence of transglutaminase. *Food Hydrocoll.* **52**, 942–951 (2016).
183. Brownlow, S. et al. Bovine β-lactoglobulin at 1.8 Å resolution — still an enigmatic lipocalin. *Structure* **5**, 481–495 (1997).
184. Weiss, M. S., Palm, G. J. & Hilgenfeld, R. Crystallization, structure solution and refinement of hen egg-white lysozyme at pH 8.0 in the presence of MPD. *Acta Crystallogr. D.* **56**, 952–958 (2000).
185. Jo, S., Vargyas, M., Vasko-Szedlar, J., Roux, B. & Im, W. PBEQ-solver for online visualization of electrostatic potential of biomolecules. *Nucleic Acids Res.* **36**, W270–W275 (2008).

Acknowledgements
The authors are indebted to W. K. Fong and M. Usuelli for discussions and thank A. Diego-González for producing the mayonnaise sample reported in Fig. 1a.

Author contributions
All authors contributed to all aspects of manuscript preparation, revision and editing.

Competing interests
The authors declare no competing interests.

Publisher's note
Springer Nature remains neutral with regard to jurisdictional claims in published maps and institutional affiliations.

Reviewer information
Nature Reviews Physics thanks E. Zaccarelli, N. Brooks and the other, anonymous, reviewer(s) for their contribution to the peer review of this work.